Pfander et al. *Swiss Journal of Geosciences* (2022) 115:12
https://doi.org/10.1186/s00015-022-00414-z

SGG SGS sc | nat
Swiss Journal of Geosciences

ORIGINAL PAPER Open Access

Glaciofluvial sequences recording the Birrfeld Glaciation (MIS 5d–2) in the Bern area, Swiss Plateau

Jonathan Pfander[1*], Fritz Schlunegger[1], Elena Serra[1], Natacha Gribenski[1], Philippos Garefalakis[1,2] and Naki Akçar[1]

Abstract

In this paper, we document that glaciofluvial gravel sequences and glacial till deposits that are exposed in the Müntschemier and Finsterhennen gravel pits (Swiss Plateau west of Bern) record three glacial advances during the Birrfeld Glaciation, which corresponds to the last glacial cycle. Sedimentological logging shows that both gravel pits expose deposits of glaciofluvial braided river systems. These sediments are overlain by a till that was deposited during the Last Glacial Maximum (LGM). The results of the provenance analysis imply that the sediments were mainly supplied by the Valais Glacier, which originated in the Central Alps. A minor contribution of the material was supplied by the Saane Glacier with sources in the northern parts of the Alps. In addition, the morphometric analysis particularly of quartzite clasts in the till deposits indicate that while some clasts (the angular ones) were eroded and transported by the Valais Glacier from the Central Alps to the depositional site, the majority of the quartzite constituents (the rounded ones) were most likely reworked from the Molasse bedrock or older gravels. This implies that a large fraction of the sediments in the Müntschemier and Finsterhennen gravel pits could represent recycled material from older fluvial gravels and conglomerates that were then reworked by the glaciers as they advanced to the foreland. Based on the sedimentological data and considering published and new optically stimulated luminescence (OSL) chronological data, we propose a landscape evolution scenario where the first glacial advance occurred during Marine Isotope Stage (MIS) 5d. The second glacier advance followed during MIS 4, while the last one during the Last Glacial Maximum (LGM), which corresponds to the MIS 2. The MIS 5d advance is recorded by the lowest unit of the Müntschemier gravel pit and consists of a fining upward sequence made up of an alternation of gravel and sand beds. The MIS 4 advance is recorded by the unit beneath the LGM till at Müntschemier and by the lowermost layer in the Finsterhennen gravel pit. It comprises an alternation of gravel and sand beds, which coarsens and thickens upwards. The LGM advance, finally, resulted in the deposition of amalgamated gravel beds at Finsterhennen, which ended with the construction of a till that is encountered on the top of both gravel pits. Sediments related to the interstadial conditions between MIS 5a and MIS 5b and MIS 3 were not encountered, which suggests that the warmer periods were characterised by non-deposition and/or erosion, which possibly resulted in the observed sedimentary hiatus. Although the chronological results are still preliminary, the available information allows us to suggest that during the Birrfeld Glaciation,

Editorial handling: Wilfried Winkler.

*Correspondence: jonathan.pfander@geo.unibe.ch; jonathan.pfander@hotmail.com
[1] Institute of Geological Sciences, University of Bern, Baltzerstrasse 1+3, 3012 Bern, Switzerland
Full list of author information is available at the end of the article

the Valais lobe advanced several times to the Swiss Plateau. In addition, the facies associations imply that the eastward expansion of the Valais lobe during the MIS 5d and MIS 4 were most likely shorter than during the LGM.

1 Introduction

During the Quaternary period, the Swiss Plateau and its adjacent mountainous regions experienced at least 15 advances of Alpine glaciers (e.g., Monegato & Ravazzi, 2018; Muttoni et al., 2003; Preusser et al., 2011; Schlüchter, 1986, 2004). The history of Quaternary glacial advances into the Swiss Plateau is built on a combination of geomorphological observations, detailed logging of numerous sedimentological sections, and chronologies established by various dating techniques including 14C, surface exposure dating with terrestrial cosmogenic nuclides, and optically stimulated luminescence (OSL) (e.g., Ivy-Ochs et al., 2008; Preusser et al., 2011; Schlüchter, 2004). Among the numerous foreland glaciations, the last glacial cycle, which is locally referred to the Birrfeld Glaciation (Graf & Müller, 1999; Graf, 2009a, b), is most probably the best investigated one. During this glaciation, which spans approximately the last 120 ka, at least three glacial advances occurred in the Swiss Plateau (Ivy-Ochs et al., 2008; Preusser et al., 2007, 2011). The third and most recent one was dated to the time interval between 30 and 17.5 ka including the period between 24 and 21.5 ka when the Alpine glaciers with sources in the central part of this orogen reached their maximum extents (Ivy-Ochs et al., 2008; Preusser, 2004; Schlüchter et al., 2021). This latter glacial advance occurred during the global Last Glacial Maximum (LGM) (Shakun & Carlson, 2010), which has been correlated with the maximum in global ice volume during Marine Isotope Stage (MIS) 2 (Ivy-Ochs et al., 2008; Schlüchter, 2004). The LGM has been extensively investigated in the Alps (e.g., Bini et al., 2009; Graf et al., 2015), thanks to the clear and well preserved glacial landforms and deposits, such as moraines, erratic boulders and glaciofluvial gravels that could be related to the LGM. In contrast, except for a few chronological studies (e.g., Gaar et al., 2019; Preusser, 1999), the history of the previous Alpine glacial advances during the Birrfeld Glaciation has been less explored, mainly because of the poor preservation of the related deposits and the difficulty to access the corresponding stratigraphic archives. Nevertheless, based on lithostratigraphic evidence and the results of luminescence dating, Ivy-Ochs et al. (2008) suggested that two glacial advances occurred during MIS 5d and 4, both of which preceded the LGM.

The gravel pits at Finsterhennen and Müntschemier, which are situated in the Swiss Plateau to the northwest of Bern (FIH and MÜN on Fig. 1), offer potential sites where sedimentary archives preceding the LGM are exposed. In particular, the results of previous chronological investigations suggest that the deposition of the sediments at Finsterhennen most likely occurred in response to two glacial advances during MIS 4 and MIS 2 times (Preusser et al., 2007; Schlüchter, 2004). Therefore, it is possible that further investigations of the Finsterhennen (FIH) and Müntschemier (MÜN) gravel pits will allow us to reconstruct the early advances of the Alpine glaciers onto the Swiss Plateau during the Birrfeld Glaciation, and to compare them with the extent of the LGM glaciation (Fig. 1a). Such information has been missing so far (Preusser et al., (2011), see their Fig. 19), and we expect that the MÜN and FIH sites offer ideal archives to fill this knowledge gap. Accordingly, we logged in detail the stratigraphic sections in both gravel pits. We determined the petrographic and morphometric properties of the clasts and the paleo-flow directions at these sites in an effort to gain information on the provenance of the sediments, the dominant transport mechanisms and the depositional environment. Finally, we determined the depositional ages of a sand layer in the MÜN gravel pit through the application of the infrared stimulated luminescence (IRSL) dating technique on two feldspar samples. These ages complete the chronological record of the Birrfeld Glaciation for the MÜN and FIH ensemble, which provides geologic evidence for a further archive where material of the last glacial period is potentially preserved.

2 Study site

The gravel pits at Müntschemier (MÜN) and Finsterhennen (FIH) are situated in the Swiss Plateau ca. 20 km west of Bern and ca. 15 km southeast of the Jura Mountains (Fig. 1). The region surrounding the pits is characterised by three lakes (Biel, Neuchâtel and Murten) and a flat alluvial plane made up of peat, which extends over several kilometres (Fig. 1b). This area was affected by environmental engineering practices in the framework of two so-called "Juragewässerkorrektionen" (1868–1891 and 1962–1973), with the result that ca. 400 km^2 of peat was transformed to agricultural land (Eugster and Schneider, 2006). Seismic surveys and multiple drillings have shown that this region is underlain by several hundreds of metres-deep overdeepenings that were carved into the Molasse bedrock (Lower Freshwater Molasse and Upper Marine Molasse) by subglacial processes throughout repeated Quaternary glacial advances (Dehnert et al.,

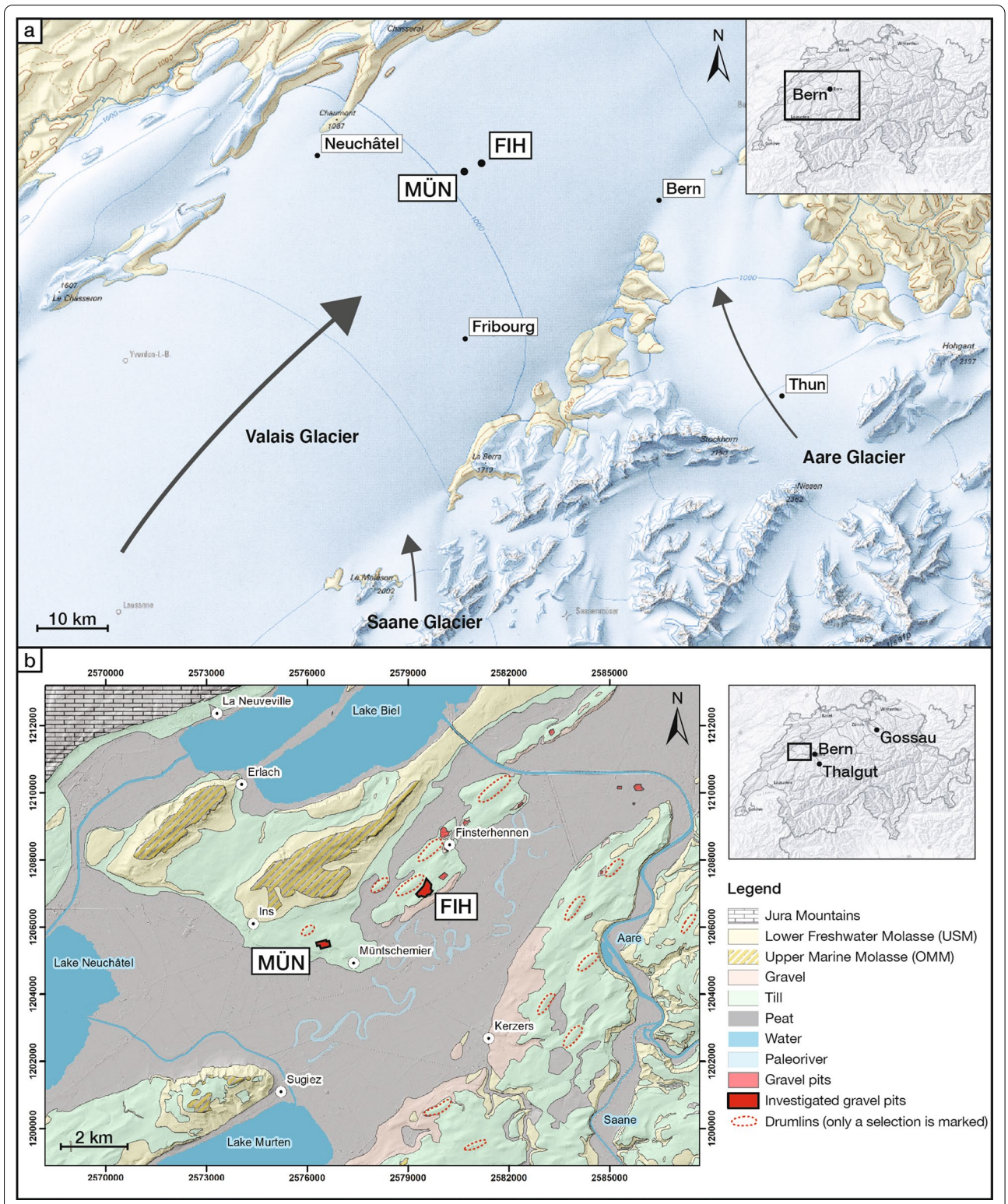

Fig. 1 Location of the gravel pits at Müntschemier (MÜN) and Finsterhennen (FIH) displayed on **a** the Last Glacial Maximum (LGM) map (Bini et al., 2009) together with the lobes of the Valais, Saane, and Aare Glaciers (© Federal Office of Topography, swisstopo, CH-3084 Wabern) and **b** the geological map

2012; Dürst Stucki & Schlunegger, 2013; Magrani et al., 2020; Reber & Schlunegger, 2016). These troughs were then filled by glacio-lacustrine sediments or host modern lakes (Dehnert et al., 2012; Buechi et al., 2017; Gegg et al., 2021; Schwenk et al., 2022). The lakes and alluvial planes are bordered by drumlins and roches moutonées that are covered by a till probably of a LGM age, and that have a SW–NE extension, which parallels the flow direction of the Valais Glacier during the LGM (Dürst Stucki & Schlunegger, 2013). This glacier was sourced in the central Alps and reached its maximum position ca. 45 km farther NE of the study area, where terminal moraines mark the position of the former ice margin (Ivy-Ochs et al., 2008). South of the study area and also during LGM times, two additional glaciers (Saane and Aare, Fig. 1a) with sources in the northern part of the Alps advanced to the Swiss Plateau and converged with the Valais Glacier near Fribourg (Saane Glacier) and Bern (Aare Glacier) (Preusser et al., 2011). The bedrock underneath the Quaternary sediments consists of Early Miocene sandstones and mudstones of the Lower Freshwater Molasse (USM) and Upper Marine Molasse (OMM).

The MÜN and FIH pits are located on one of these drumlins (Fig. 1b). They comprise a till cover that was most likely deposited during the LGM (Preusser et al., 2007). The diamicts at these sites are underlain by a sequence of sand and gravel layers that have not been dated yet (Müntschemier), and by a suite of gravels at Finsterhennen, which were already dated. In particular, a mammoth tusk, which was found embedded in pro-glacial meltwater deposits below the uppermost till layer at Finsterhennen, has an originally reported age of 25.4 ± 0.2 ^{14}C ka BP (Schlüchter, 2004), which was then corrected to an age of 29.5 ± 0.6 ka (cal.) BP using a more recent ^{14}C calibration (Graf et al., 2015). This age assignment was then complemented by two OSL ages of 28.5 ± 2.3 ka and 28.9 ± 2.5 ka within the same glaciofluvial unit (Preusser et al., 2007). Consequently, the pro-glacial meltwater deposits and the overlying till at this site have been attributed to the LGM glaciation (Preusser et al., 2007). In addition, OSL dating of glaciofluvial sediments below a till in the lower part of the same gravel pit yielded an age of 76.0 ± 6.0 ka (Preusser et al., 2007), which suggests that these sediments were possibly associated with an earlier glacial advance into the lowlands during MIS 4 (Ivy-Ochs et al., 2008; Preusser et al., 2007, 2011). Because of ongoing gravel mining, the sites for which these ages were determined in the Finsterhennen gravel pit do no longer exist, and precise information about where the chronological samples were taken is not available, unfortunately.

3 Methods

We used several methods including techniques in sedimentology and geochronology to reconstruct the depositional processes, the sedimentary environments, and the evolution of the landscape in this part of the Swiss Plateau.

3.1 Remote sensing

High-resolution digital elevation models of the MÜN (Fig. 2a) and FIH (Fig. 2b) gravel pits were generated to

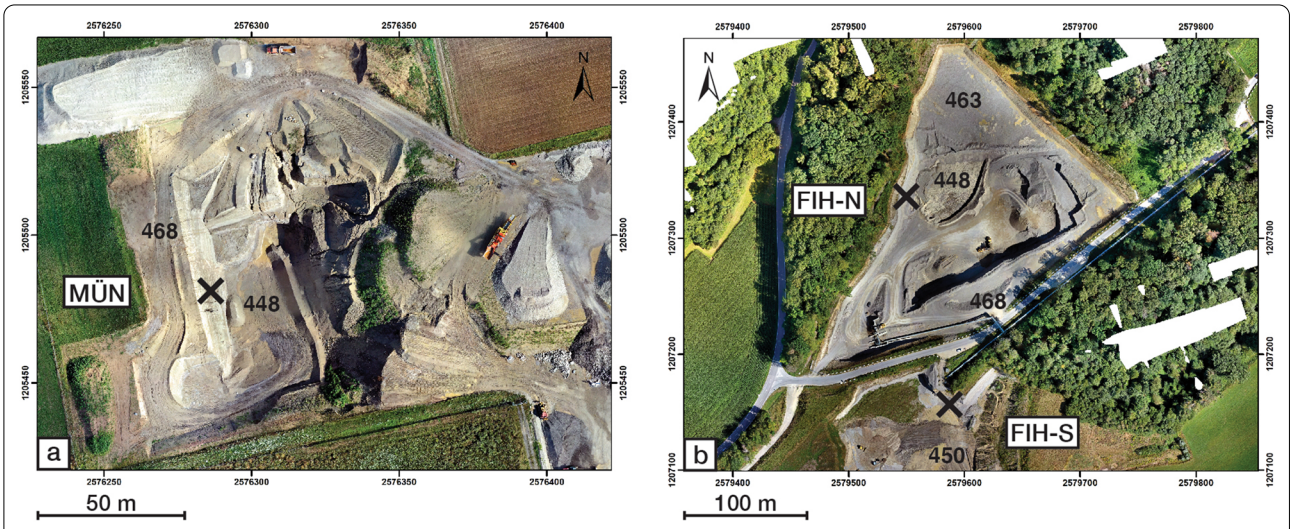

Fig. 2 Orthomosaic high-resolution pictures of the gravel pits at **a** Müntschemier (MÜN) and **b** Finsterhennen southern (FIH-S) and northern part (FIH-N). Crosses indicate the location of the sedimentological logs illustrated in Figs. 5, 6, and 7 (see these figures for coordinates of sections), and the numbers show the elevation in metres above sea level

gain an overview of the investigation area, to allocate the sections for the subsequent logging, and to precisely determine the location where the sedimentological logs were taken. Such an allocation is required because the sections will disappear as gravel mining proceeds. The aerial photographs were taken with the unmanned air vehicle (or drone) DJI Mavic 2 Pro®. These images then served the basis to generate, for each gravel pit, a high-resolution orthomosaic (2.4 cm/pix and 2.07 cm/pix, for MÜN and FIH respectively). This was accomplished through combining a total of 253 and 716 images that were taken at MÜN and FIH, respectively with the software Agisoft Metashape Professional®.

3.2 Sedimentological analysis

3.2.1 Facies description and logging

Sedimentological logging of the sediments at Müntschemier and Finsterhennen (sites indicated with crosses on Fig. 2) was accomplished following the scheme proposed by Evans and Benn (2014) and Buechi et al. (2017). The larger gravel pit (FIH) is subdivided into a northern (FIH-N, 19.5 m thick) and a southern section (FIH-S, 18.0 m thick), while in the smaller gravel pit (MÜN) only one section was logged (20 m thick). For each of these three sections, in-situ observations and digital images were used to collect data on grain size, to identify the sedimentary structures and to measure the thicknesses of individual units, as well as to determine paleo-flow directions (see below). The results of sedimentological analyses are used to identify 11 different lithofacies elements (or lithofacies, LF; Table 1), which are grouped into 5 lithofacies associations (LFA; Table 2) in an effort to reconstruct the depositional paleo-environments following Rust (1978), Miall (1985), Buechi et al. (2017) and Schwenk et al. (2022). The occurrence of these lithofacies associations (LFA) was then used as a basis to develop a scenario of how the landscape of the study area evolved through time.

3.2.2 Paleo-flow direction analysis

The orientation of elongated and flat pebbles in alluvial sediments can be used to infer the paleo-flow direction at the time of deposition (Krumbein, 1939; Rust, 1972). This can be accomplished by measuring either the azimuth of the longest a-axis of an elongated clast, or the azimuth of the a-b-plane of disc-shaped or flat pebbles (Krumbein, 1939; Millane et al., 2006; Rust, 1972) where the b-axis is the clast's intermediate axis. For elongated clasts, it is important to note that the orientation of the a-axis depends on the transport mechanism. In particular, if such pebbles bounce upon transport, they tend to be deposited with their a-axis parallel to the flow (e.g. Schlee, 1957), while rolling on the bed surface results in an orientation where the a-axis is aligned perpendicular to the flow (e.g. Doeglas, 1962; Kelling & Williams, 1967), which is commonly the case in a fluvial setting (Johansson, 1963; Millane et al., 2006). In a till, however, the long (a-) axis of elongated clasts is oriented parallel to the ice flow (Evans & Benn, 2014; Nichols, 2009).

For disc-shaped or flat pebbles, the a-b-plane tends to be orientated dipping upstream, resulting in imbrication (Doeglas, 1962; Johansson, 1963; Kauffman & Ritter, 1981; Millane et al., 2006; Nichols, 2009; Rust, 1972; Schlunegger & Garefalakis, 2018). Because orientations of a-b-planes of flat pebbles yield generally a more consistent picture on the paleo-flow direction than measurements of the a-axes of elongated pebbles (Millane et al., 2006), we preferentially conducted our measurements on flat pebbles particularly for fluvial gravels. Furthermore, because the orientation of smaller clasts largely depends on the transport and deposition of the larger clasts (Potter & Pettijohn, 1977), only the larger clasts (i.e. > mean grain size) are considered for our measurements. Please note that we avoided measuring the orientation of those clasts that occur in cross-bedded layers because pebbles are lying flat on the bedform surface in such deposits, which could add a bias. The paleo-flow dataset was then complemented by information provided by orientations of cross-beds, which also allow to determine the directions of the paleo-flow at the time of sediment accumulation (Nichols, 2009). All measurements were conducted with a compass in the field.

3.2.3 Pebble petrography

Investigations on the pebble petrography are an important part of the provenance analysis of sediments as the resulting information can be used to determine the source area of the sediments (e.g., Claude et al., 2017a; Graf & Müller, 1999; Graf et al., 2015; Meichtry, 2016). In addition, such data bear information on the transport, erosion, weathering, sorting and recycling mechanisms prior to deposition (Schlüchter, 1989; Weltje & von Eynatten, 2004). In this context, special attention is focussed on identifying the key lithologies because they indicate a spatially constrained source area (e.g., Claude et al., 2017b, 2019). We followed the analysis protocol provided by Claude et al. (2017a) and randomly collected 250 pebbles within 4 m^2-large areas along the sections at MÜN and FIH using a bucket. The pebbles were then grouped into the following lithological classes using a hammer, HCL (3.2%), and macroscopic criteria: Vein quartz, quartzite, granite and metamorphic rock (granite, gneiss and crystalline schist, and amphibolite), serpentinite and green crystalline, sandstone, dark-coloured limestone (dark-coloured limestone and siliceous limestone), light-coloured limestone (light- and flesh-coloured limestone

Table 1 Lithofacies elements, related abbreviations, and descriptions of their properties

Lithofacies	Abbreviation	Description	Interpretation
Massive diamict	Dmm	Silt to boulders, unsorted, matrix-supported, 1–5 m thick beds Clasts: Sub-angular to sub-rounded, sometimes broken, some striations visible Matrix: Brown-beige silty fine sand, massive, unstratified	Subglacial till[a]
	Dmm-1	Same structures as Dmm, additionally enriched with quartzite, granite and metamorphic pebbles, gradual basal contacts	
	Dmm-2	Same structures as Dmm, additionally enriched with limestones, sharp basal contacts	
Massive gravels	Gm	Medium-grained sand to boulders, massive, poorly sorted, mostly grain-supported, few sand lenses, sharp basal contact, 0.5–2 m thick beds Clasts: Sub-angular to well-rounded Matrix: Greyish medium to coarse sand	Longitudinal bars[b]
Cross-bedded gravels	Gc	Fine-grained sand to boulders, cross-bedded, moderately sorted, normal and inverse grading, grain and matrix-supported, sharp basal contact, 0.3–1.5 m thick beds Clasts: Sub-angular to well-rounded Matrix: Greyish fine- to coarse-grained sand, sometimes washed out	Longitudinal bars and channel fills[b]
Massive sand	Sm	Fine- and medium-grained sand, massive, medium-sorted, 0.1–1.5 m thick beds	Planar bed flows[b]
Horizontally bedded sand	Sh	Fine- and medium-grained sand, horizontally bedded (mm-scale), well-sorted, normal and inverse grading, sharp basal contact, 0.1–0.5 m thick beds	Planar bed flows[b]
Cross-bedded sand	Sc	Fine- to coarse-grained sand, few gravels, cross-bedded, medium-sorted, normal grading, sharp basal contact, 0.1–0.5 m thick beds	Scour fills, transverse bars, longitudinal bars, sand waves[b]
Laminated and sheared sand and fines	SFl(s)	Clay to medium-grained sand, laminated, sheared, brown-beige colour, sharp basal contact, 1–1.5 m thick bed, underlying Dmm-2	Deformed pro-/sub-glacial deposits[c]
Laminated fines	Fl	Silt and clay, fine lamination interbedded with minor fine-grained sand, well-sorted, sharp basal contact, max. 2 cm thick beds	Overbank deposits[b]

F Fines (silt and clay), *l* laminated; *S* Sand, *m* massive, *h* horizontally bedded, *c* cross-bedded, *G* Gravel, *m* massive, *c*: cross-bedded, *Dm* Diamict, matrix-supported, *m* massive, *(s)* sheared

After Miall (1977), van der Meer (1993) and Evans and Benn (2014)

[a] Evans et al. (2006)

[b] Miall (1977)

[c] van der Meer (1993)

Table 2 Summary of the lithofacies associations. Interpretation of depositional environment is based on Miall (1978) and Buechi et al. (2017)

Lithofacies associations	Lithofacies	Description	Interpretation
LFA 1	Gm, Gc, Sm, Sh, Sc	Alternation of gravel and sand beds, fining upward	Braided river, development from proximal to distal[a]
LFA 2	Sm, Sh, Sc	Amalgamation of sand beds	Braided river, distal[a]
LFA 3	Gm, Gc, Sh, Sc, Fl	Alternation of gravel and sand beds, coarsening upward	Braided river, development from distal to proximal[a]
LFA 4	Gm, Gc,	Amalgamation of gravel beds, coarsening upward	Proximal braided river[a]
LFA 5	Dmm-1 or Dmm-2, SFl(s)	Matrix-supported diamict with a high contribution of quartzite, granite and gneiss pebbles (Dmm-1) or dark limestone pebbles (Dmm-2). Sometimes deformed sand and fines (SFl(s) underlies Dmm-2	Glacial till of the MIS 2 glacier and glacio-tectonised sand and fines[b]

[a] Miall (1978)

[b] Buechi et al. (2017)

and oosparite), Niesen- and Gurnigel-Flysch, and others (volcanic rock, conglomerate, claystone, and unknown) (Table 3 and Fig. 3). Please note that there are more advanced ways of determining the clast composition of gravels (Schiemenz, 1960). We justify the use of our simple approach since it is sufficiently well suited to identify first order patterns and changes of the petrographic composition of coarse-grained deposits, which is the scope of our paper (e.g., Schlunegger et al., 1993).

3.2.4 Pebble morphometry

The shape of pebbles provides information about the transport mechanisms (e.g., fluvial versus glacial), the depositional environment, and particularly about the origin of the clasts (e.g. Claude et al., 2017a; Lukas et al., 2013; Schlüchter, 1989). In the context of the material's provenance, it has been reported that rounded quartzite pebbles represent products of reworked fluvial sediments such as the Miocene Molasse conglomerates or older unconsolidated gravels, whereas sub-angular pebbles are interpreted to indicate rather fresh erosional products from the Alps (e.g. Claude et al., 2017a; Du Pasquier, 1891). In our case, sub-angular quartzite pebbles are likely to represent clasts that were eroded from the St. Bernard nappe in the Central Alps (Spicher, 1972) and transported by the Valais Glacier to the study area. We thus selected quartzite clasts for the morphometric analysis because of their abundance in the gravel pits and because research on the relationships between their morphometry and transport mechanisms has already been conducted (see above). We collected 100 quartzite pebbles from multiple 4 m^2-large outcrops and determined the pebble morphometry by calculating the roundness (Zi) (1) and flattening (Ai) index (2):

$$Zi = \frac{2r}{L} \times 1000 \tag{1}$$

and

$$Ai = \frac{L + w}{2E} \times 100 \tag{2}$$

where L is the length, w the width, E the thickness of the pebble and $2r$ the smallest curvature radius in the L/w

Table 3 Summary of the lithological classes, their description, and main source after Gerth and Becker-Haumann (2007)

Lithological class	Description	Main Source
Vein quartz	White quartz grains, medium- to coarse-grained, partly dark enclaves (Fig. 3a)	Widespread
Quartzite	White-yellowish to dark, granular texture, fine- to medium-grained, a schistosity is sometimes visible (Fig. 3b)	St. Bernard nappe
Granite and metamorphic rock	*Granite:* Colourful and medium-grained (Fig. 3c), light and fine-grained, or reddish and fine- to medium-grained (Fig. 3d) *Gneiss and crystalline schist:* Foliation at a mm- to cm-scale, alternating layers composed of light and dark bands (Fig. 3e, f) *Amphibolite:* Metamorphic rock with dark amphiboles and light feldspar, medium-grained (Fig. 3g)	External massifs
Serpentinite and green crystalline	Green serpentine, magnetic, and other greenish lithologies (Fig. 3h)	Zermatt-Saas Fee unit
Sandstone	Colourful (Fig. 3i), dark (Fig. 3j), or beige, fine- to medium-grained, reacts with HCL 3.2%	Widespread
Dark-coloured limestone	*Dark-coloured limestone:* Dark, micritic-sparitic, fine veins, reacts strongly with HCL 3.2% (Fig. 3k) *Siliceous limestone:* Dark, micritic, reacts weakly with HCL 3.2%, scratches the hammer	Helvetic nappes, Penninic sedimentary nappes
Light-coloured limestone	*Light- and flesh-coloured limestone:* Beige-reddish, micritic, veins, reacts strongly with HCL 3.2% (Fig. 3l) *Oosparite:* 1–3 mm-large ooids, grain supported, reacts with HCL 3.2% (Fig. 3m)	Penninic sedimentary nappes, Jura Mountains
Niesen- and Gurnigel-Flysch	Colourful breccia, angular components of different size, orange weathered dolomite grains (Fig. 3n, o)	Penninic Flysch
Others	*Volcanic rock:* Phenocrysts in a fine-grained matrix, matrix supported, different colours *Conglomerate:* Various rounded clasts in a fine-grained matrix *Claystone:* Reddish—dark, soft *Unknown:* Pebble cannot be assigned to a lithology	Molasse conglomerates, Molasse units, widespread

Note that all clast types could also have been derived through reworking of Miocene Molasse conglomerates or older Quaternary gravels. Here, we list the possible original source areas (i.e., prior to reworking)

Fig. 3 Cut and polished pebbles from the Müntschemier and Finsterhennen pits. **a** Vein quartz, **b** Quartzite, **c**, **d** Granite, **e**, **f** Gneiss, **g** Amphibolite, **h** Serpentinite, **i**, **j** Sandstone, **k** Dark-coloured limestone, **l** Light-coloured limestone, **m** Oosparite, and **n**, **o** Niesen- and Gurnigel-Flysch

plane, respectively (Cailleux, 1947). Here, low *Zi* values indicate angular pebbles, whereas high values are characteristic for rounded pebbles. Likewise, low *Ai* values point to spheroidal pebbles, and high values represent elongated and flat pebbles (Schlüchter, 1989).

The resulting *Zi* and *Ai* values were grouped into bins with an interval of 50 following Schlüchter (1989). These large groups also consider the uncertainties, which are usually associated upon estimating the required radii of the pebbles from the measured variables. From this dataset, we then created an *Ai–Zi* plot following Schlüchter (1976) to infer a possible glacial or fluvial imprint on the shape of the clasts and thus the origin of the material (Fig. 9).

3.3 Luminescence dating

Because the deposits at MÜN have not been dated yet, we determined a depositional age using optically stimulated luminescence (OSL) dating technique (Aitken, 1998). Two samples referred to as GUG20-01 and GUG20-02 were collected in black plastic tubes from the top and the bottom of a ca. 5.5 m-thick unit of amalgamated sand beds (LFA 2; Fig. 4a). Samples were prepared under red light laboratory conditions at the Institute of Geological Science, University of Bern. The 150–200 µm-size fraction, which was then used for luminescence measurements, was extracted by wet sieving. The samples were treated with 10% HCl and 30% H_2O_2 to remove carbonates and organic components, respectively. After chemical treatment, density separation was performed with heavy liquid LST (sodium heteropolytungstate solution) to isolate quartz and feldspar minerals (density of 2.70 and 2.58 g/cm^3 for quartz and feldspar, respectively). Quartz separates were etched with HF (40% for 1 hour) but were not used for further analyses due to the dim luminescence signal and the high feldspar contamination that was revealed by preliminary quartz OSL measurements. Feldspar grains were fixed on 10 mm diameter stainless steel discs using a silicon spray and a 1-mm aliquot mask.

Luminescence measurements were conducted with a TL/OSL DA-20 Risø reader equipped with a calibrated $^{90}Sr/^{90}Y$ beta source at the Institute of Geology, University of Bern. Feldspar infrared (IR) stimulation of 1-mm aliquots was performed with IR LEDs emitting at 875 nm. The generated luminescence signal (called infrared stimulated luminescence, IRSL) was detected in the blue wavelength by the photomultiplier tube EMI 9235QA with a Schott BG-39 and L.O.T.-Oriel D410/30 nm filter combination.

Equivalent doses (D_e) were measured for each 1 mm aliquot (n = 24 per sample) using a post-IR IRSL 150 °C protocol similar to the one of Reimann and Tsukamoto (2012). In this $pIRIR_{150}$ protocol, a preheat at 180 °C is followed by a first IRSL stimulation at 50 °C (IR_{50}) and a second post-IRSL stimulation at 150 °C ($pIRIR_{150}$). The suitability of the $pIRIR_{150}$ protocol was assessed with dose-recovery and residual tests (Wintle & Murray, 2006), carried out on samples that were previously bleached under sunlight. After removing the residual signals, recovery ratios were within 10% of unity for all the samples. For data analysis, IRSL signals were integrated over the first 1.2–10 s minus the last 90–99 s, and dose–response curves were constructed using exponential fitting. Acceptance criteria for each individual aliquot measurement data include a recycling ratio within 15% of unity and a recuperation within 10% of the natural dose.

Final D_e per sample used for the age calculation was determined using the Central Age Model (CAM; Galbraith & Roberts, 2012) or the Finite Mixture Model (FMM; Galbraith & Green, 1990). We selected the FMM model for the case where the overdispersion (OD) of the measured 1 mm-aliquot D_e distribution was significantly larger than the reported OD values for well bleached (i.e. fully reset luminescence signal prior to deposition) glacio-fluvial deposits in the Alps with similar measurements (OD ~ 19%, Gaar et al., 2014). The FMM was run using multiple components (testing 2 to 4 components) with sigma-b values (σ_b, which corresponds to expected OD for well-bleached sample) of 0.2 (Gaar et al., 2019).

Finally, the D_e values that resulted from the CAM or FMM models were then corrected for fading (i.e. spontaneous loss of feldspar luminescence signal with time; Wintle, 1973) using fading rates measured on the same aliquots as those that were used for D_e measurements. This was accomplished following Auclair et al. (2003) and by applying the fading correction procedure of Huntley and Lamothe (2001), which is implemented in the Luminescence R package developed by Kreutzer et al. (2012).

U, Th, and K concentrations, which were used for the determination of the environmental dose rate, were measured on the bulk sediment collected around the target samples. The measurements were conducted using high-resolution gamma spectrometry (Department of Chemistry and Biochemistry, University of Bern, Switzerland; Preusser et al., 2001). The resulting radionuclide concentrations, an assumed water content of 10 ± 5%, an internal K-content of 12.5 ± 0.5% (Huntley & Baril, 1997), and an alpha efficiency value of 0.15 ± 0.05 (Balescu & Lamothe, 1994) were then considered upon employing the Dose Rate and Age Calculator (DRAC) by Durcan et al. (2015). The ages were obtained by dividing the

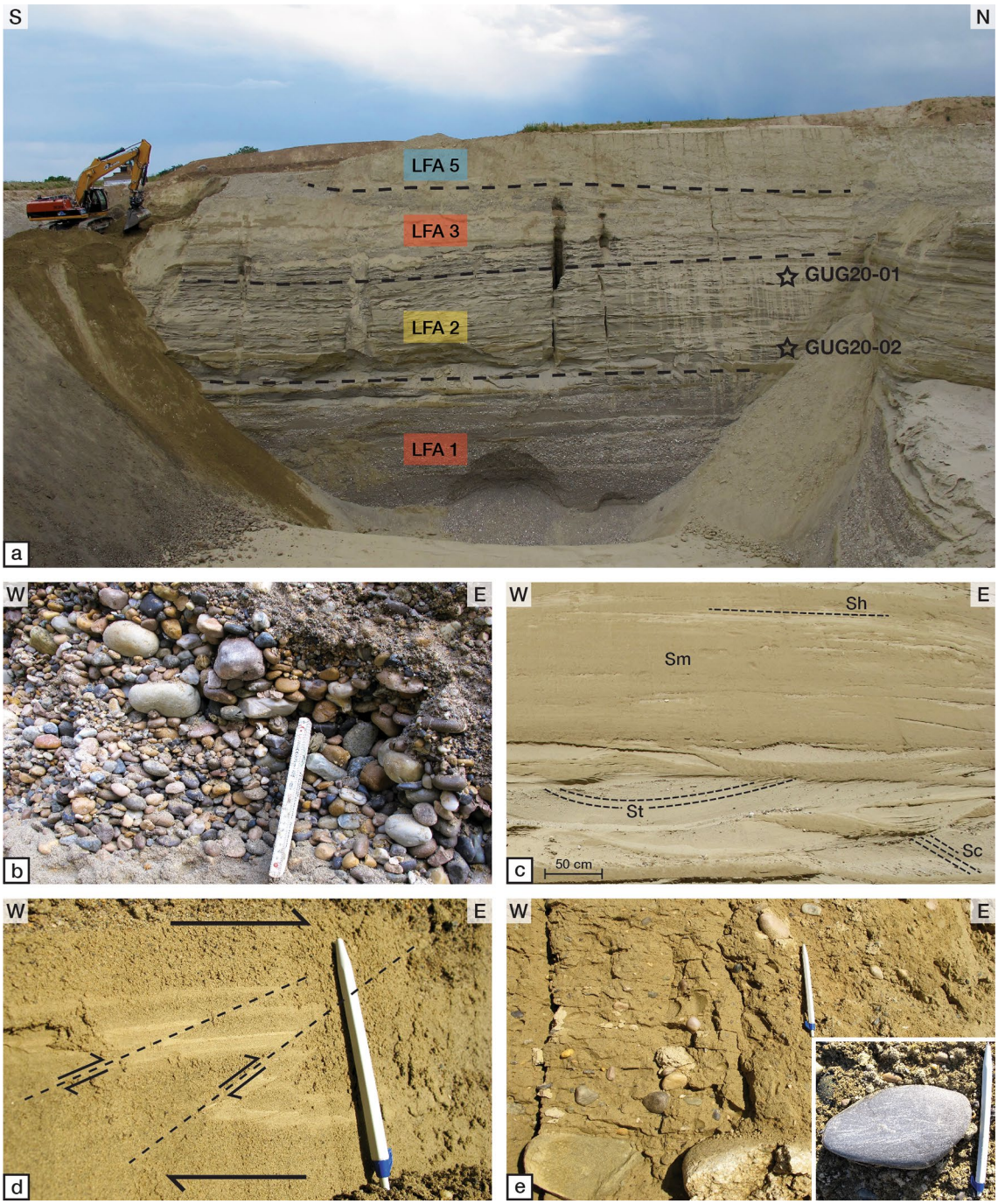

Fig. 4 **a** Succession at the MÜN pit including photos of the lithofacies associations: LFA 1—Alternation of gravel and sand beds, fining upward; LFA 2—Amalgamation of sand beds with projected locations of IRSL samples GUG20-01 and GUG20-02; LFA 3—Alternation of gravel and sand beds, coarsening upward; and LFA 5—Matrix-supported diamict enriched in quartzite, granite, and metamorphic pebbles. **b** Grain-supported gravel bed of LFA 1 with few crushed pebbles. **c** Amalgamation of massive, horizontally bedded, and cross-bedded sand beds (Sm, Sh, and Sc (St: trough-cross-bedded); Table 2) in LFA 2. **d** Sheard silt and clay layer in a sand bed in the lower part of LFA 3. **e** Pebbles and boulders embedded in a silt and sand matrix represent the diamict of LFA 5. Bottom right: Polished, striated, and bullet-shaped dark limestone

fading corrected final CAM/FMM D_e by the calculated dose rate.

4 Results

4.1 Lithofacies and facies associations

The MÜN and FIH gravel pits comprise well-sorted gravel and sand beds (Fig. 4). They are overlain by ca. 2–5 m thick diamicts that have a poor sorting. The contact with the underlying Molasse bedrock is not observed in both gravel pits. The gravel and sand beds are dominated by horizontal- and cross-beddings as well as by massive structures. In general, the sediments at MÜN (Fig. 5) are mainly characterised by the occurrence of sand beds, whereas the sediments at FIH predominantly comprise medium- and coarse-grained gravel beds (Figs. 6, 7). The 11 lithofacies (LF) elements, which were identified in these sections (Table 1), were then grouped into 5 lithofacies associations (LFA, numbered from bottom to top), which are summarised in Table 2 and described with more details regarding their vertical stacking in the following chapters.

4.1.1 LFA 1—Alternation of gravel and sand beds, fining upward

Lithofacies association 1 (LFA 1) consists of an alternation of massive and cross-bedded gravel layers (Gm and Gc; Table 2) and massive- and horizontal- as well as cross-bedded sand units (Sm, Sh, and Sc; Table 2). It is only found in the MÜN gravel pit (Fig. 5). In the lower part, the gravel beds are coarse-grained and have a thickness of approximately 1.5 m. Towards the top of the LFA 1 succession, the grain size and the thickness of individual beds decrease to fine-grained gravel beds that are few decimetres thick. The fabric is mostly clast-supported. The matrix consists of grey-coloured medium- to coarse-grained sand, and only a few crushed pebbles are observed (Fig. 4b). Furthermore, some metres-wide and several decimetres-thick lenses consisting mostly of medium- to coarse-grained sand are interbedded within the gravels. While these sand beds forming horizontal layers are rare in the lower part of LFA 1, their thickness and frequency increase towards the upper part of LFA 1. This trend is also associated with a general fining-upward trend (Fig. 5). Measurements of the orientation of clasts and cross-beds (a total of 70) indicate a transport direction towards the NE to S albeit with a large spread.

The results of the petrological investigations reveal that the clast suite of LFA 1 is dominated by (i) light-coloured (32%) and dark-coloured (15%) limestone clasts, (ii) quartzite constituents (19%), and (iii) granite and metamorphic rocks (16%). The roundness index values (*Zi*) of quartzite pebbles range between 50 and 750. They have a median value of ca. 340. Lower values (angular shape) are rare in comparison to the higher values (rounded shape). The flattening index values (*Ai*) of the same pebbles have a median of 157 (Fig. 5).

4.1.2 LFA 2—Amalgamation of sand beds

Lithofacies association 2 (LFA 2) consists of an amalgamation of massive- and horizontal- as well as cross-bedded sand layers (Sm, Sh, and Sc; Table 2) (Fig. 4c). This LFA is encountered in the middle of the MÜN section (Fig. 5) and at the base of the FIH gravel pit in its northern part (Fig. 6). At both sites, the bed thickness varies between the centimetre- to the metre-scale. The beds mainly consist of fine- to medium-grained sand with a low amount of silt. In general, they are brownish-beige-coloured. Few gravel beds are embedded preferentially in Sc at the bottom and the top of LFA 2. The contacts to the underlying LFA 1 and the overlying LFA 3 are gradual. No paleo-flow and morphometric data was collected for this LFA.

4.1.3 LFA 3—Alternation of gravel and sand beds, coarsening upward

Lithofacies association 3 (LFA 3), which occurs in both gravel pits (Figs. 5, 6, 7), consists of an alternation of massive and cross-bedded gravel beds that have a clast- and matrix-supported fabric (Gm and Gc; Table 2). At both sites, decimetre-thick horizontal- and cross-bedded sand interbeds (Sh and Sc; Table 2) and a few centimetres-thick laminated clay layers also occur (Fl; Table 2). These fine-grained sediments are mainly interbedded within the sand beds. In the lower part of LFA 3, gravel beds are rare, thin (approximately 20 cm), and dominated by fine-grained clasts. This lower part is thus characterised by the occurrence of fine- and medium-grained, cross-bedded sand layers that are > 1 m thick. Towards the upper part of LFA 3, the thickness of the gravel beds increases to 0.5–1.5 m, whereas the sand layers thin to between 0.5 and 1 m. LFA 3 can thus be characterised by a coarsening upward trend particularly at FIH-S. The beds of LFA 3 are often affected by deformation features such as dykes consisting of clay fillings, clay pebbles, and faults. Figure 4d shows the occurrence of a thrust fault at the centimetre-scale at MÜN, which indicates an E-directed paleo-shear movement. Measurements of the orientation of clasts and cross-beds indicate a large spread in flow directions that are mainly oriented towards the NE.

The results of the petrological investigations reveal that whereas the clast types in LFA 3 are the same at the three sites (MÜN, FIH-N and FIH-S) and similar to LFA 1, their relative abundance is quite different, particularly if the LFA 3 clast composition at the three sites is compared with each other. For instance, quartzite clasts

contribute to > 25% to the clast suite at MÜN and 18% at FIH-N (Figs. 5, 6), but they are less frequent at FIH-S (9%; Fig. 7). In the same sense, whereas dark-coloured limestone clasts contribute to 40% at FIH-S (Fig. 7), their abundance is ca. 20% at FIH-N and MÜN (Figs. 5, 6) and thus ca. 50% less than in FIH-S. In general, the clast composition of the LFA 3 unit is remarkably different between both FIH sections (Figs. 6, 7), but similar between FIH-N and MÜN (Figs. 5, 6). In the same sense, the distribution of clast types is similar between LFA 3 and LFA 4 at FIH-S (Fig. 7), but different between LFA 3 and LFA 4 at FIH-N (Fig. 6). As will be pointed out in the discussion, this pattern complicates a stratigraphic correlation between the sections.

Within LFA 3, the median of the roundness index values (*Zi*) measured for the quartzite clasts ranges between 250 (FIH-S) and ca. 315 (MÜN, FIH-N), which is thus slightly lower than in LFA 1. The median of the flattening index *Ai* values is ca. 155 for all sites, which is the same as in LFA 1.

4.1.4 LFA 4—Amalgamation of gravel beds, coarsening upward

Lithofacies association 4 (LFA 4), which is only encountered at FIH (Figs. 6, 7), consists of an amalgamation of massive and cross-bedded gravel layers that coarsen upward (Gm and Gc; Table 2). The sedimentary structures of the gravel beds vary with the orientation of the outcrops and the location of observations. In general, the lower part is dominated by medium-sized gravel beds, while towards the upper part, the dominant grain size changes to coarse-grained gravels. Occasionally boulders with diameters up to 30 cm occur within this unit. The fabric is mostly clast-supported, and some pebbles are crushed. The matrix consists of medium- to coarse-grained sand. Rarely the matrix is completely washed out. A few metres-wide and few decimetre-thick sand lenses occur in the lower and middle part of LFA 4. The contact to the underlying LFA 3 is erosional, and the depths of the erosional scours vary laterally at the decimetre-scale. The contact to the overlying LFA 5 is sharp and

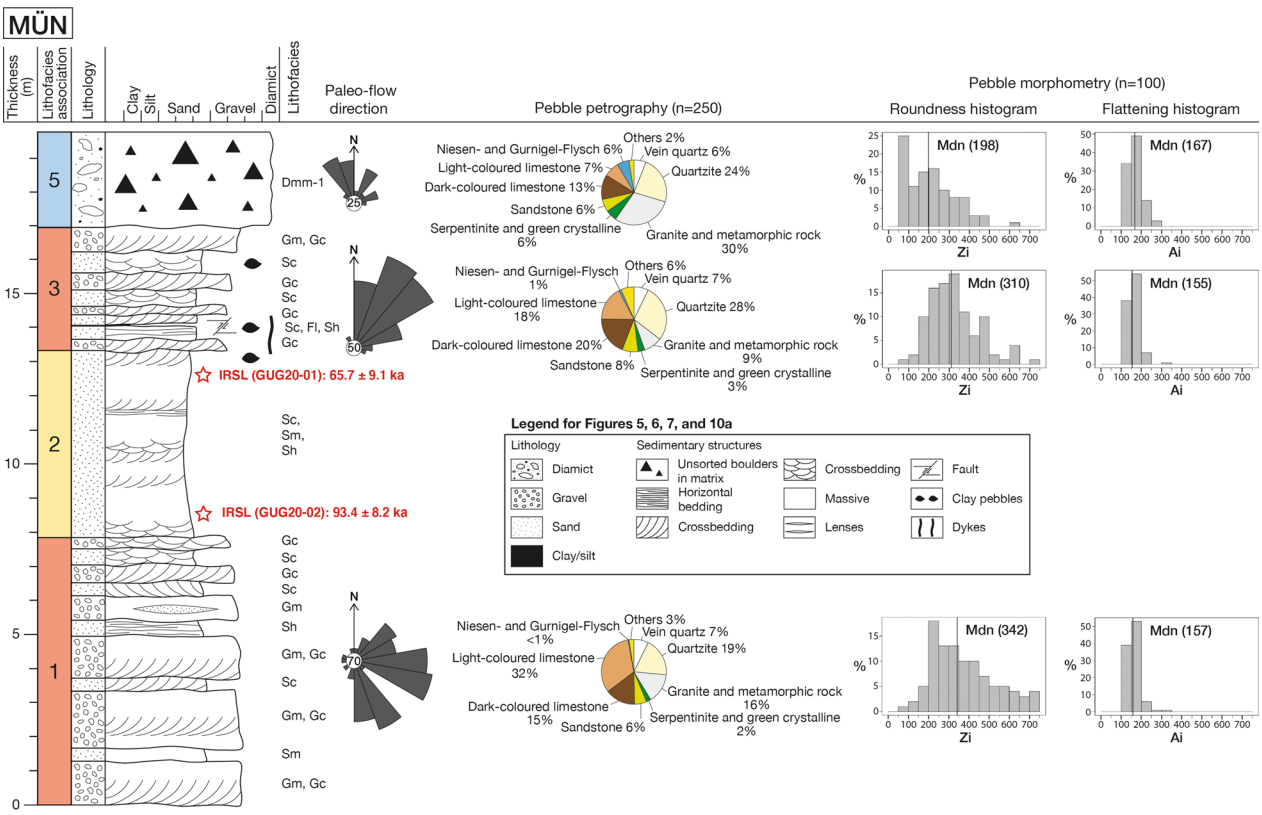

Fig. 5 Sedimentological log of sediments recorded at Müntschemier (MÜN; section situated at CH1903 + /LV 95: 2′576′282.1, 1′205′472.4; top of LFA 5 at 468.6 m a.s.l.) with (i) lithofacies associations (LFA; Table 2), lithofacies (LF; Table 1), projected IRSL (red star: GUG-20–01 and GUG20-02), (ii) paleo-flow directions, (iii) pebble petrography, and (iv) pebble morphometry. See Fig. 2 for location of the log

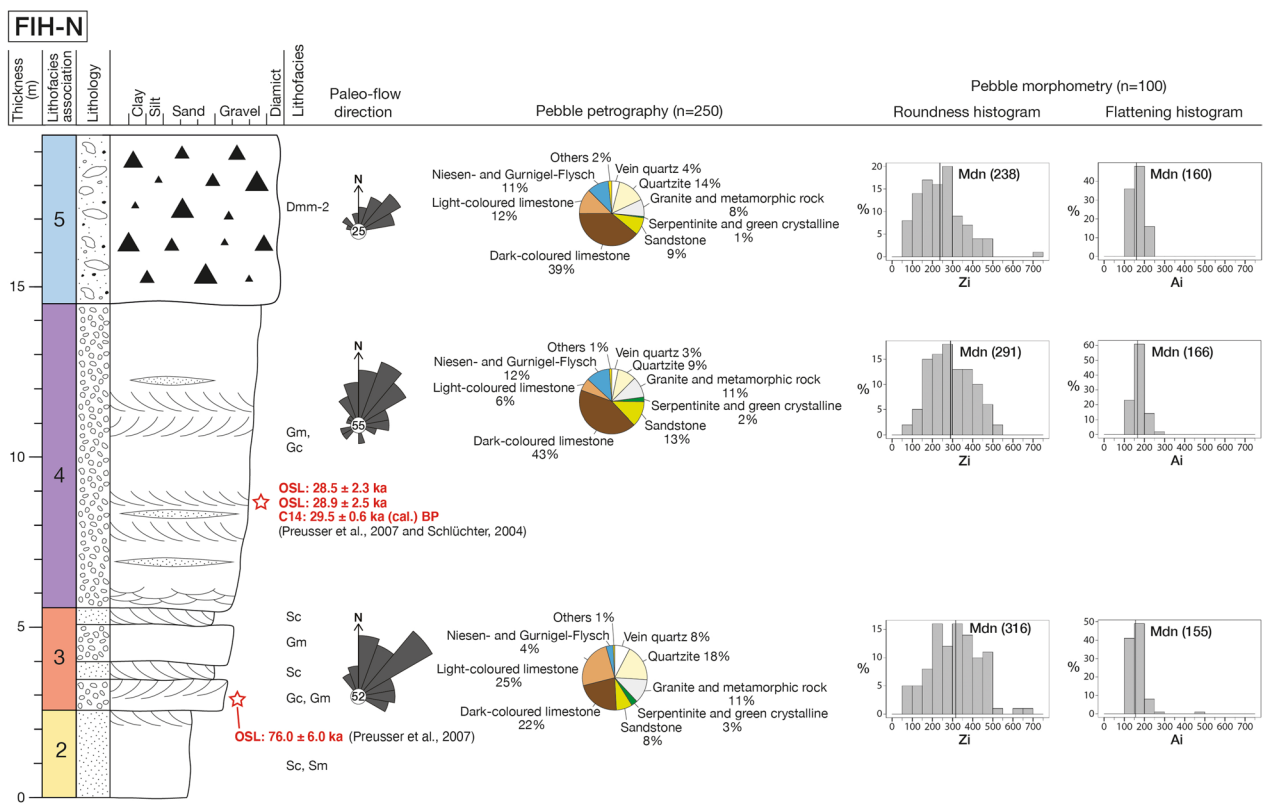

Fig. 6 Sedimentological log shows the sedimentary record at Finsterhennen northern part (FIH-N; CH1903 + / LV 95: 2′579′541.1, 1′207′329.8, top of LFA 5 at 466.8 m a.s.l.) with (i) lithofacies associations (LFA; Table 2), lithofacies (LF; Table 1), (ii) paleo-flow directions, (iii) pebble petrography, and (iv) pebble morphometry. Published OSL and radiocarbon (C14) ages are projected into the section and indicated as red stars. See Fig. 2 for the location of the log, and Fig. 5 for the legend

characterised by a horizontal plane. Measurements of the orientation of clasts point to a paleo-flow direction that was generally oriented towards the N with a large spread between W and E. A small population of paleo-flow data even points towards the SW.

The results of the petrological investigations reveal that the clast types in LFA 4 are identical at both FIH sections. Limestone clasts clearly dominate the petrographic composition (ca. 50%), followed by ca. 20% of sandstone constituents (including Flysch clasts). The other clast types include quartzite, igneous and metamorphic lithologies. Interestingly, whereas the clast suite of LFA 4 is similar to that in LFA 3 at FIH-S (Fig. 7), it is quite different to the LFA 3 unit in FIH-N (Fig. 6; see also section above).

Similar to LFA 3, the distribution of the roundness index (*Zi*) values of the quartzite clasts reveals a large spread between 50 and 600. The mean *Zi* ranges between ca. 250 (FIH-S) and ca. 290 (FIH-N), which is nearly the same as in LFA 3 at FIH-S (250), but smaller than in LFA 3 at FIH-N (ca. 315) and at MÜN (310), and also smaller than in LFA 1 (ca. 340). The flattening index values (*Ai*) of the same pebbles reveal a median value Mdn (*Ai*) of 159 and 166, which is comparable to LFAs 1 and 3.

4.1.5 LFA 5—Matrix-supported diamict

Lithofacies association 5 (LFA 5) represents the uppermost layer in all sections and consists of an unsorted and matrix-supported diamict (Dmm; Table 2), which is partially underlain by a sheared sand and clay bed (Sfl(s); Table 2). The thickness of LFA 5 varies spatially between 2 and 5 m. The Dmm consists of pebbles, cobbles, and up to 40 cm large boulders, which are embedded in a brown-beige-coloured silty and sandy matrix (Fig. 4e). The colour of this matrix thus contrasts to the grey colour of the underlying LFA 3 and LFA 4 deposits at MÜN and FIH, respectively. The contact of LFA 5 to the underlying units is sharp. In some places, these sediments show faults at the mm-scale, which indicate a paleo-shear movement. Polished, striated, and elongated clasts can be found in the scree deposits in front of the outcrop (Fig. 4e). Such pebbles were most probably transported by a glacier (Boulton, 1978). Finally, the orientation of the clasts

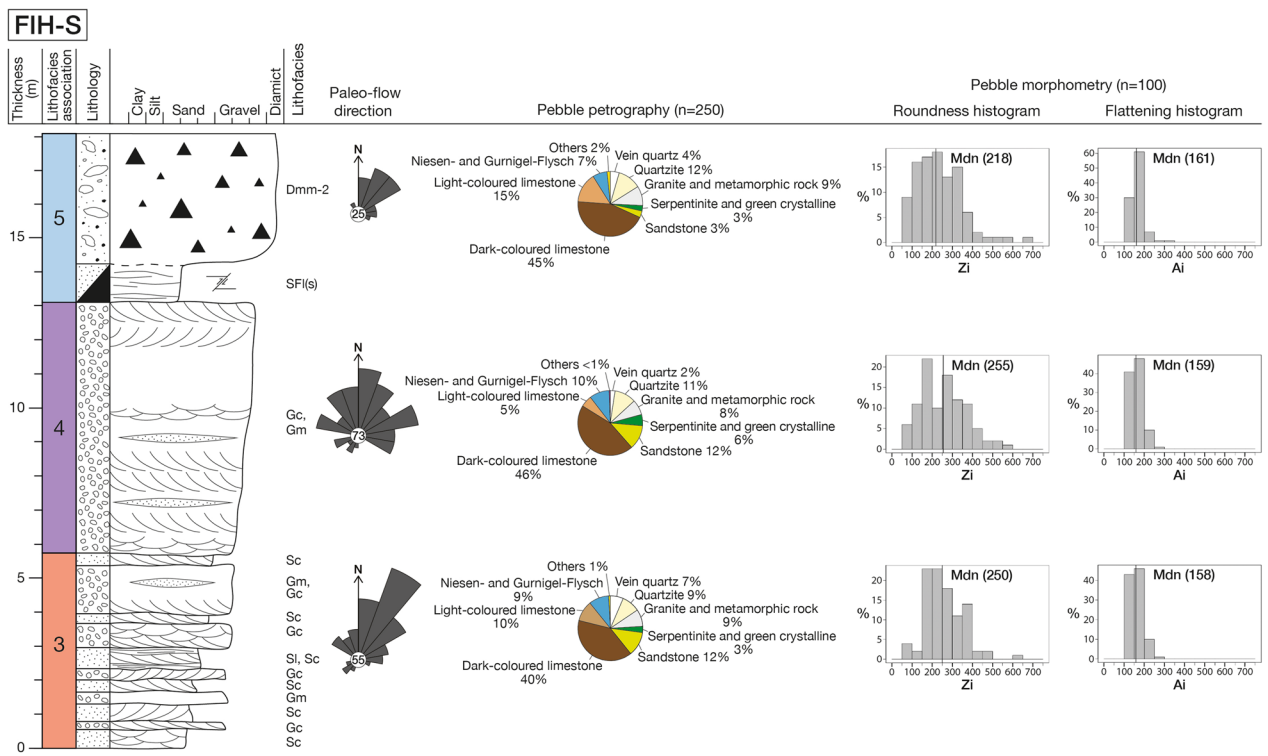

Fig. 7 Sedimentological log shows the sedimentary record at Finsterhennen southern part (FIH-S; CH1903 + / LV 95: 2′579′589.4, 1′207′160.1, top of LFA 5 situated at 466.1 m a.s.l.) with (i) lithofacies associations (LFA; Table 2), lithofacies (LF; Table 1), (ii) paleo-flow directions, (iii) pebble petrography, and (iv) pebble morphometry. See Fig. 2 for the location of the log, and Fig. 5 for the legend

suggests that the paleo-transport occurred towards the NNW (MÜN) and the NE (FIH-N and FIH-S).

The results of the clast counts reveal that the LFA 5 petrographic composition at MÜN is dominated by granite and metamorphic clasts (30%), followed by quartzite components (24%) and limestone lithologies (20%). This composition is quite different to the LFA 5 at FIH, where the clast suite is dominated by limestone constituents at both sites (ca. 50–60%), followed by sandstone and flysch clasts (10–20%) and quartzite components (between 10 and 15%). The other clast types include igneous and metamorphic lithologies including serpentinite clasts.

The distribution of the roundness index values (*Zi*) of the quartzite clasts reveals a large spread that ranges between 50 and nearly 700. The median of the *Zi* values clusters between ca. 200 and 240 at the three sites, which is the lowest value that was determined for the sediments at these sites. Similar to the other LFAs, the flattening index values (*Ai*) of the same pebbles have a median Mdn (*Ai*) of around 160.

4.2 Luminescence dating

The results of feldspar IR_{50} and $pIRIR_{150}$ measurements (1-mm aliquots) of samples GUG20-01 and GUG20-02 that were collected from unit LFA 2 at MÜN are summarised in Table 4 and Fig. 8. They show that for sample GUG20-01, 1 mm- aliquot D_e distributions for both signals are multimodal and significantly dispersed (OD values of 27.8% for IR_{50} and 30.7% for $pIRIR_{150}$) compared to similar well-bleached glaciofluvial deposits investigated in the Alps (OD ~ 19%, Gaar et al., 2014). For both signals, the calculated D_e using the FMM model results in a moderate decrease (< 15%) of the final D_e that is obtained through applying the CAM model. Final ages calculated from FMM D_e and corrected for fading are 65.7 ± 9.1 (IR_{50}) and 112.3 ± 9.5 ka ($pIRIR_{150}$). Distributions of 1 mm- aliquot D_e for sample GUG20-02 are moderately dispersed (OD around 20% for both IR_{50} and $pIRIR_{150}$ measurements). Fading-corrected ages from calculated CAM D_e are 93.4 ± 8.2 ka (IR_{50}) and 144 ± 11.0 ka ($pIRIR_{150}$).

Table 4 Details of luminescence dating conducted on 1 mm-aliquots of GUG20-01 and GUG20-02, using feldspar IR_{50} and $pIRIR_{150}$ signals

Sample	Radionuclide concentration			Total dose rate (Gy ka^{-1})	Nr. of aliquots	CAM Uncorr D_e (Gy)	OD (%)	FMM Uncorr De (Gy)	g_{2days} (%/decade)	CAM* or FMM fading corr. D_e (Gy)	Age (ka)
	U (ppm)	Th (ppm)	K (%)								
IR_{50}											
GUG20-01	1.7 ± 0.1	5.5 ± 0.1	1.3 ± 0.0	2.2 ± 0.1	24	119.1 ± 6.9	27.8	104.1 ± 8.0	2.8 ± 0.8	141.3 ± 18.6	65.7 ± 9.1
GUG20-02	1.6 ± 0.3	4.7 ± 0.1	1.3 ± 0.0	2.0 ± 0.1	24	128.5 ± 5.3	19.5	/	3.4 ± 0.4	189.3 ± 14.1*	93.4 ± 8.2*
$pIRIR_{150}$											
GUG20-01	1.7 ± 0.1	5.5 ± 0.1	1.3 ± 0.0	2.2 ± 0.1	23	256.2 ± 16.7	30.7	220.0 ± 13.6	1.0 ± 0.4	241.5 ± 17.6	112.3 ± 9.5
GUG20-02	1.6 ± 0.3	4.7 ± 0.1	1.3 ± 0.0	2.0 ± 0.1	24	252.6 ± 11.9	22.4	/	1.4 ± 0.3	292.8 ± 17.6*	144.5 ± 11.0*

Sample locations: GUG20-01 (CH1903 + / LV 95: 2′576′280.0, 1′205′535.0, 7 m depth below surface) and GUG20-02 (CH1903 + / LV 95: 2′576′312.5, 1′205′516.3, 11 m depth below surface)

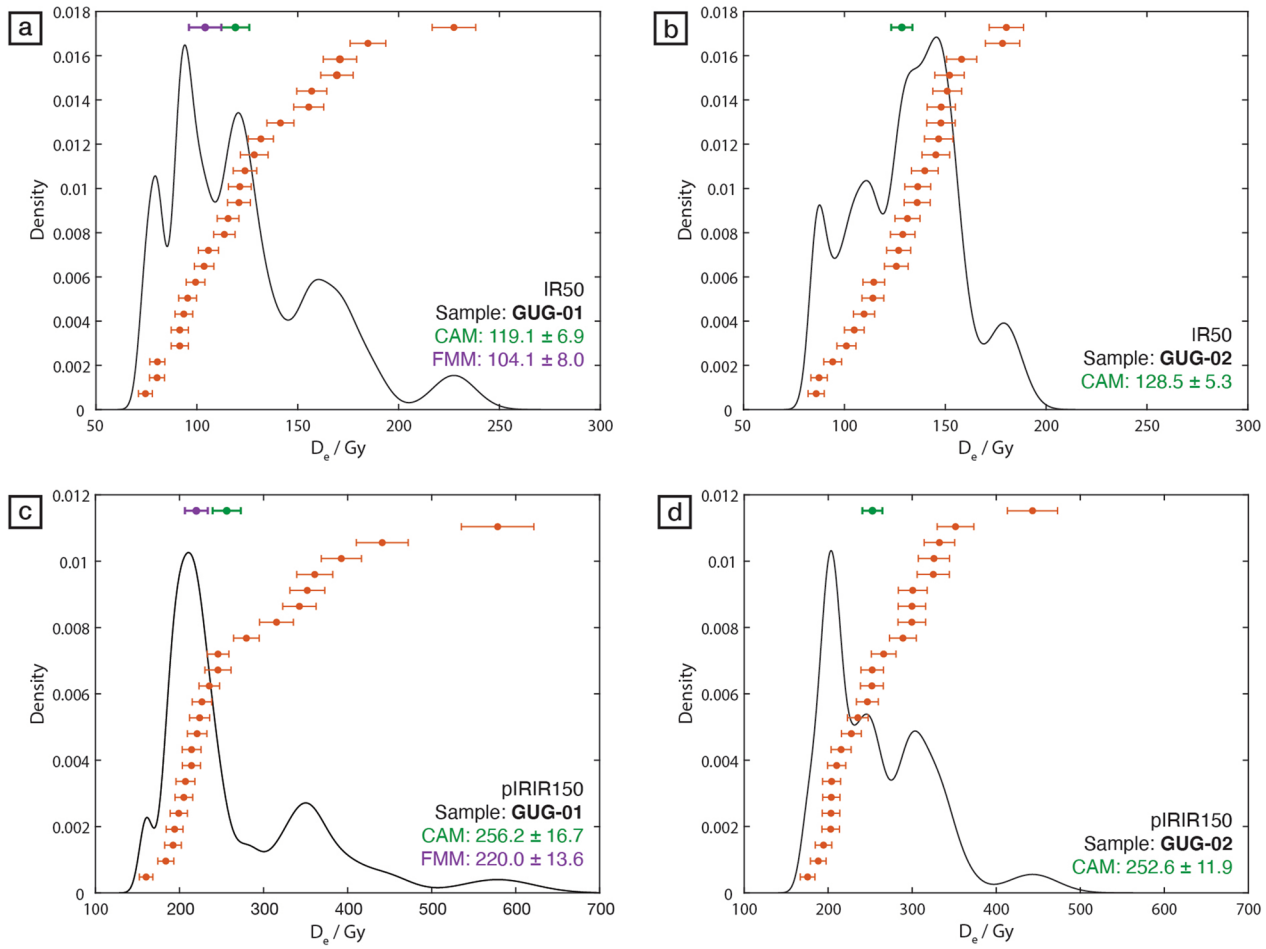

Fig. 8 Density plot of the uncorrected luminescence D_e distribution of sample GUG20-01 (**a** and **c**: IR_{50} and $pIRIR_{150}$ measurements, respectively) and GUG20-02 (**b** and **d**: IR_{50} and $pIRIR_{150}$ measurements, respectively). D_e obtained by applying the CAM and FMM (only for GUG20-01) on the D_e distributions are shown in green and purple, respectively

The large difference between final fading corrected IR_{50} and $pIRIR_{150}$ ages for both samples (ratio $IR_{50}/pIRIR_{150}$ ages of ~ 0.59 for GUG20-01, and ~ 0.65 for GUG20-02) suggest that the $pIRIR_{150}$ signal, at least, is significantly affected by partial bleaching (i.e. limited exposure to light prior to deposition), due to its lower resetting properties compared to the IR_{50} signal (Kars et al., 2014). We therefore focus for the rest of the discussion only on the FMM (for GUG20-01) and CAM (for GUG20-02) fading corrected IR_{50} depositional ages (i.e., 65.7 ± 9.1 ka and 93.4 ± 8.2 ka, respectively).

5 Interpretation of sedimentary environments

5.1 Lithofacies association LFA 1: braided river system with a trend from a proximal towards a more distal setting

LFA 1 is encountered at MÜN only, where the related sediments are interpreted to have been deposited by a braided river system within a glaciofluvial environment. In such a setting, a large proportion of the gravelly bedload is transported by rolling and saltation along the channel bed, which results in the formation of longitudinal and transverse gravel bars with massive to cross-bedded structures (Miall, 1978; Nichols, 2009). In general, the gravel deposits are products of high-water stages, during which high-energy conditions prevail, whereas the sandy components are deposited during the waning stages of a flood. The structures of the sand beds display evidence for planar bed flow, scour fills, longitudinal bars, transverse bars, sand waves and dunes (Table 1; Miall, 1978). The fining upward trend of LFA 1 is interpreted to record a transition from large runoff with high-energy conditions to a lower waterflow with less transport energies. The crushed pebbles within the grain supported sections most likely resulted from high stress conditions at the grain to grain contact during

the subglacial deformation at any time after deposition (van der Meer, 1993). The large spread of the paleo-flow directions is typical for a braided river system (Nichols, 2009). The median of the roundness index (Mdn (Zi) = 342) established for the quartzite clasts suggests that this facies association contains the roundest pebbles that were encountered in the investigated sediments and, therefore, reflects the largest fluvial signal in comparison to the other gravel containing LFAs (Fig. 9).

5.2 Lithofacies association LFA 2: braided river system with a distal sediment source

LFA 2 is encountered both at MÜN and in the northern segment at FIH (i.e. FIH-N). This unit exposes sedimentary features that are diagnostic for a low energy braided river system, which was possibly sourced at some distance from the MÜN and FIH-N sites. We base this interpretation on the distinct assemblage of lithofacies elements and their sedimentary properties (Tables 1, 2). In particular, the structures encountered in LFA 2, which are characterised by the occurrence of planar beds, point to the deposition in the upper flow regime. Additionally, features that are indicative for scour fills, longitudinal bars, transverse bars, dunes, and sand waves are also found (Miall, 1978). Because LFA 2 mainly comprises coarse- and medium-grained sand, the sediment source (most likely the front of a glacier, see below) was situated farther away from the study area compared to the other LFAs where the material comprises much coarser material.

5.3 Lithofacies association LFA 3: braided river system with a trend from a distal towards a more proximal sediment source

Similar to the lowermost LFA 1, LFA 3 is interpreted to have been deposited by a braided river, possibly in a glaciofluvial environment. The gravel beds are considered as products of longitudinal bars, gravel bars, and channel fills (Miall, 1978; Nichols, 2009), and the cross-bedded sand layers probably represent scour fills and transverse bars. In addition, upper flow regime conditions might have contributed to the formation of planar beds (Miall, 1978). The coarsening upward trend encountered in this LFA is interpreted as evidence towards a decreasing distance from the material source. This is thus the major difference to LFA 1, which shows a fining- and thinning-upward trend, suggesting an increasing distance to the material source. The centimetre-thick laminated clay layer in the lower part of LFA 3 at MÜN could be interpreted as overbank deposits (Miall, 1978). Also at MÜN, the centimetre-scale thrust fault is interpreted as a result of glaciotectonic deformation, induced by the pressure and shear stress of an advancing glacier (Hart & Boulton, 1991).

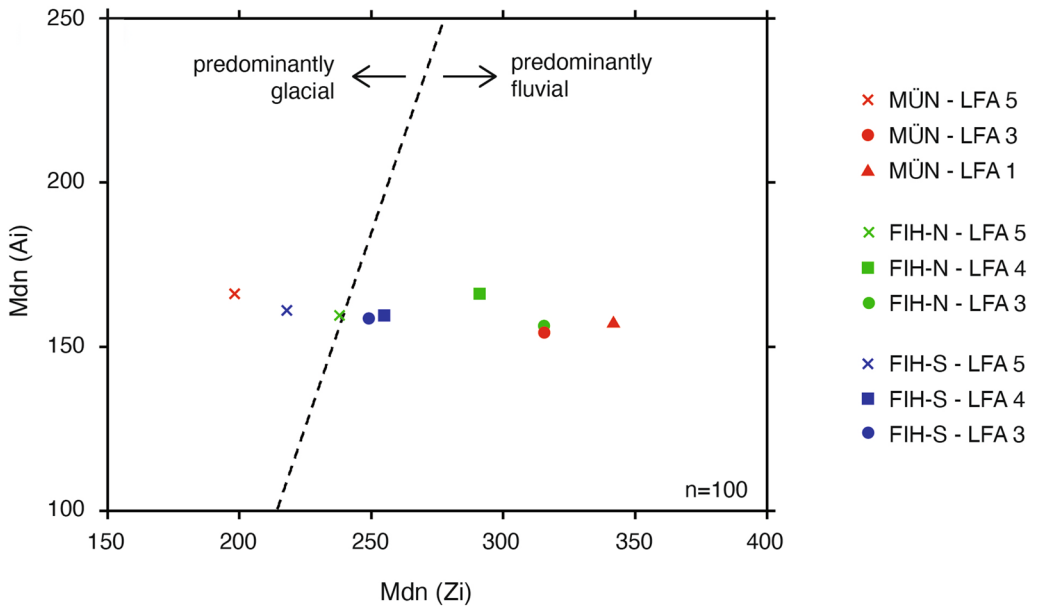

Fig. 9 *Ai–Zi* plot showing the median values of the flattening (*Ai*) and roundness indexes (*Zi*) of quartzite clasts collected at MÜN, FIH-S, and FIH-N. Low *Zi* values = angular pebbles, high *Zi* values = rounded pebbles, low *Ai* values = spheroidal pebbles, and high *Ai* values = elongated/ flat pebbles. After Schlüchter (1976)

5.4 Lithofacies association LFA 4: braided river system close to a glacier's front

LFA 4 is interpreted as a deposit of a braided river close to a glacier's front. This interpretation is based on the predominantly massive structure and clast-supported fabric of the coarse-grained material that additionally coarsens upward, thus pointing towards a decreasing distance to the sediment source (Miall, 1977, 1985). This suggests a short transport distance and a possible material supply from a glacier (Etienne et al., 2003). In addition, the large spread of the paleo-flow directions is characteristic for a braided river system (Nichols, 2009). Crushed pebbles within the grain supported fabric indicate high stress conditions during subglacial deformation (van der Meer, 1993), hence, the glaciofluvial sediments were overridden by the Valais Glacier after deposition (Preusser et al., 2007).

5.5 Lithofacies association LFA 5: till

The diamict layers encountered in LFA 5 are interpreted as glacial till. This interpretation is corroborated by the occurrence of a matrix-supported fabric and by the roundness data, which indicates that most pebbles have an angular and sub-angular shape, thus pointing to a transport predominantly by a glacier. In addition, the lower part of the LFA 5 at FIH-S bears evidence for glaciotectonic deformation. Because such deformation is not encountered at the other sites, the occurrence of such a feature might vary spatially. The transport direction and thus the ice flow was oriented towards the NE and thus parallel to the long axis of the roche moutonnées (Dürst Stucki & Schlunegger, 2013) and the orientation of the Swiss Plateau.

6 Discussion

6.1 IRSL ages

The IRSL ages established for LFA 2 at MÜN have to be considered with caution. Indeed, the significant difference (~ 30–40%) between the IR_{50} and $pIRIR_{150}$ ages for both samples after fading correction suggests a moderate time of exposure to light before the sediments were deposited, which is typically the case in a glaciofluvial environment (Fuchs & Owen, 2008). Furthermore, although we used the signal with the best bleaching properties (IR_{50}) for the final age calculation and despite the fact that we employed the FMM model to isolate the best bleached sub-population of the D_e measurements, we cannot exclude the persistence of an inherited signal in our measurements. If such as signal would occur, it cannot be isolated at the measurement scale (i.e. 1 mm aliquot) that is applied in this work. Considering these aspects, the IRSL ages that we obtained for the sand layers at MÜN might possibly represent an overestimate and would require further confirmation using alternative approaches (e.g., measurements at the single grain scale; e.g. Gribenski et al., 2021) or independent dating techniques (e.g. radiocarbon) if possible. Nevertheless, because the IRSL ages established for the LFA 2 sand layer at MÜN are consistent with the lithostratigraphic framework (see section 6.2) and the results of previous chronologies established for the gravely sequences at FIH, we tentatively use them for our interpretation.

6.2 Correlation of sections

The correlation between the FIH und MÜN sections is accomplished based on lithostratigraphic and chronological evidence. From a lithostratigraphic perspective, we correlate the suite with sand layers at the base of the northern FIH gravel pit, which is assigned to LFA 2 in this work, with the sandy unit in the middle of the MÜN section, which corresponds to the identical facies and thus to the same LFA (Fig. 10a). Such a lithostratigraphic correlation is justified by the position of this LFA in both gravel pits and based on the chronological constraints. First, at FIH, the top of LFA 2 is encountered at an elevation of ca. 450 m a.s.l.. At MÜN, the top of the same LFA occurs at an elevation that is ca. 10 m higher. If we consider a general sediment transport direction towards the NE, as revealed by the paleo-flow data of the under- and overlying units (Figs. 5, 6, 7), then an elevation difference of ca. 10 m over a downstream length of ca. 3.5 km yields a gradient (ca. 0.2°). Second, our IRSL data imply an age of 93.4 ± 8.2 ka and 65.7 ± 9.1 ka for the base and the top of LFA 2 at MÜN, respectively, which is consistent (within errors) with the OSL age of 76.0 ± 6.0 ka (Preusser et al., 2007) established for the base of the FIH gravels.

The interpretation of the litho- and chronostratigraphic position of LFA 3, however, is less straightforward if we consider the petrographic and morphometric data. In particular, the LFA 3 of FIH-N reveals a clast suite that is different to the LFA 3 unit in the southern part of the FIH gravel pit, but quite similar to the LFA 3 at MÜN. In contrast, at FIH-S the LFA 3 reveals a petrographic composition that is comparable to the overlying gravels that we assigned to LFA 4. Based on these observations, we tentatively group the LFA 3 unit at FIH-S with the overlying LFA 4 gravels (Fig. 10a). In contrast, the LFA 3 at FIH-N could be an equivalent to the identical unit at MÜN. These lithostratigraphic correlations have further implications for the assignment of the OSL (Preusser et al., 2007) and ^{14}C ages (Schlüchter, 2004) to one of these units, mainly because we cannot precisely locate the sample sites of these authors based on published information.

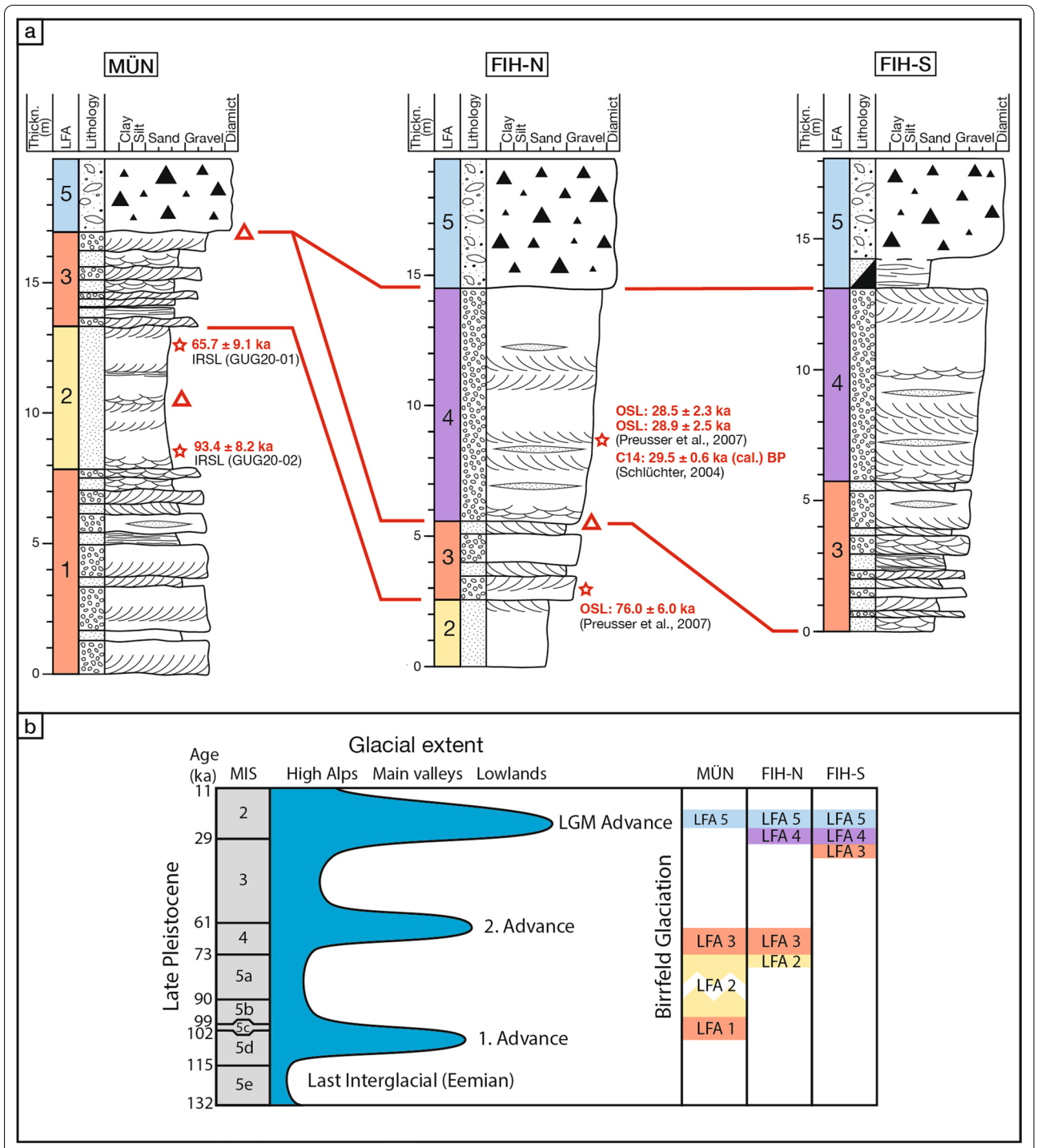

Fig. 10 **a** Correlation of the sedimentological logs at Müntschemier (MÜN; Fig. 5), the northern part of Finsterhennen (FIH-N; Fig. 6), and the southern part of Finsterhennen (FIH-S; Fig. 7). Ages are projected and indicated as red stars and possible hiatus as red triangle. See Fig. 2 for location of logs, and Fig. 5 for legend. **b** Possible timing and ice extents of three glacial advances during the last glacial cycle (Birrfeld Glaciation, modified from Ivy-Ochs et al. (2008)) and correlated with the lithofacies associations (LFA) recorded at Müntschemier and Finsterhennen. The first and second advance possibly reached the study area. The LGM advance was more extensive and covered this area with several hundred metres of ice (Bini et al., 2009). The Marine Isotope Stage boundaries are taken from Martinson et al. (1987) and Shackleton et al. (2002)

Nevertheless, based on the position of these sites relative to the glacial till, and because the LFA 3 gravels of FIH-N are more similar to the LFA 3 at MÜN than at FIH-S, we tentatively consider (i) the OSL age of 76.0 ± 6.0 ka by Preusser et al. (2007) to chronicle the accumulation of the LFA 3 at FIH-N, and (ii) the ca. 30 ka-old ^{14}C and OSL ages by Preusser et al. (2007) and Schlüchter (2004) to calibrate the deposition of the LFA 4 (Fig. 10a).

Finally, the chronological constraints allow us to assign the till LFA 5 at FIH to the LGM. As a consequence, the till at MÜN was most likely also formed during the LGM because it underlies a drumlin that has a same shape and occurs at the same elevation as the drumlin at FIH (Fig. 1b). We acknowledge that the clast composition of LFA 5 at MÜN is different to the petrographic composition of the FIH tills particularly if we consider the relative abundance of quartzites and granites/metamorphic clasts (54% at MÜN and ca. 21–22% only at FIH). In fact, because the clast compositions of the till deposits at both sites are quite similar to those of the underlying gravel units (LFA 4 at FIH-S and FIH-N, and LFA 3 at MÜN), it is possible that the petrographic composition of the LGM tills was largely achieved through erosion of the underlying gravel units with some admixture of fresh material from the Central Alps.

6.3 Origin of the material

The allocation of the origin of the clasts in the gravel pits is not straightforward because the material could have been derived from the Alps and the Jura Mountains through erosion by e.g., a glacier. Alternatively, and possibly more likely, a very large fraction of the clastic material particularly in LFA 1, 3, and 4 could have been derived either through erosion of Miocene Molasse conglomerates, or through recycling of older Quaternary gravels, all of which share similar petrographic compositions (e.g., Matter, 1964; Schlüchter, 1976). Yet, the occurrence of angular quartzite and serpentinite clasts in the till deposits (LFA 5) that overlay the gravels at both pits does point towards the Valais Glacier as an important sediment source. In this context, we can use the morphometric properties such as the roundness values of quartzite clasts as a proxy for estimating either a relative distance to the glacier's front or a relative importance of recycling of older gravelly units on the construction of the LFAs. This is the case because a high *Zi*-value, which indicates a high roundness and thus a high textural maturity of the clasts, implies a relatively long fluvial transport time and/or a low admixture of glaciogenic material, whereas a low *Zi*-value results from a clast population where the fluvial transport time is short and/or admixture of glaciogenic material is significant, thereby resulting in a low textural maturity. Accordingly, the highest mean *Zi*-value that we determined for the oldest LFA 1 unit suggests a high textural maturity where a large portion of the clasts was probably recycled from older gravels, or where the distance to the glacier's front was the largest of all gravelly units encountered in this study. In either case, the high textural maturity of the LFA 1 clasts points towards the lowest glacial signal in comparison to the overlying gravelly units. However, because the LFA 2 mainly consists of sand, the glacial signal recorded by these deposits is even less.

The nearly identical mean *Zi*-values that we determined for the quartzite clasts for the LFA 3 gravels at FIH-N and MÜN confirms the lithostratigraphic correlation where both units were possibly deposited at the same time at ca. 65–75 ka. At both sites, the LFA 3 unit chronicles a situation where the distance to the glacier's front was probably significant, yet shorter than during deposition of the LFA 1, or where a very large portion of the material was recycled from older gravel deposits. The situation then changed during deposition of the pre-LGM gravels of LFA 3 and 4 at FIH-S and LFA 4 at FIH-N where the relative admixture of angular quartzite clasts increased, finally resulting in a composition of clasts where the largest portion was supplied by a glacier as recorded by the low mean *Zi*-values of the youngest LFAs.

In summary, based on the morphometric properties of the clasts (Fig. 9) and the correlation of the sections (Fig. 10a), we assign the lowest glacial signal to the oldest gravel unit (LFA 1) that has an age older than ca. 95 ka. The subsequent package of gravel layers, which was deposited at ca. 65–75 ka and which includes the LFA 3 at FIH-N and MÜN, records evidence for a glacial signal more pronounced than at ca. 95 ka but significantly lower than during pre-LGM and LGM times between ca. 30 and 20 ka. This time span is recorded by the LFA 3 and LFA 4 units at FIH-S and by the LFA 4 gravels at FIH-N, and finally by the till deposits overlying both sites (Fig. 10a). This interpretation is consistent with the conclusion by Preusser et al. (2007) who considered the material of these LFAs to have been mainly supplied by the Valais Glacier. Furthermore, the occurence of Niesen- and Gurnigel-Flysch point to a minor sediment supply by the Saane Glacier.

6.4 Evolution of sedimentary environment

The fining upward trend of the lowermost unit LFA 1 (MÜN) is interpreted to reflect a retreat of the sediment and water source, which was possibly a glacier. We infer such a source because a large sediment flux and a large water runoff was required to transport and accumulate coarse-grained material in such a braided fluvial

environment (Miall, 1985; Rust, 1978). In addition, since the water and sediment transport occurred towards the NE, it is very likely that the sourcing ice was the Valais Glacier, which advanced to the Swiss Plateau most likely during MIS 5d (Fig. 10b) as the IRSL age of 93.4 ± 8.2 ka in the overlying sandy unit (LFA 2) suggests. Because the transition to the overlying LFA 2 unit is characterised by a continuous fining-upward trend, we infer that the LFA 1 to LFA 2 succession records the retreating stage of this glacier and the transition to a warmer period. Accordingly, we consider LFA 1 to record the first glacial advance of the Birrfeld Glaciation (Fig. 10b).

The age interval between the base (93.4 ± 8.2 ka) and the top of the LFA 2 (65.7 ± 9.1 ka) spans approximately 30 ka and is thus quite long. This time span also corresponds to the time interval between ca. MIS 5c and MIS 5a, during which, except for MIS 5b, warmer conditions prevailed (Helmens, 2014; Wohlfarth, 2013). These age constraints thus suggest that LFA 2 chronicles a period with low sedimentation and/or erosion. This interpretation is consistent with the inferences by Dehnert et al. (2012), who dated lake sediments and peat material in the Wehntal overdeepening (north of Zürich, Switzerland) with luminescence dating and palynology. Based on the resulting age pattern, the aforementioned authors considered the occurrence of a sedimentary hiatus during MIS 5a in their sedimentary succession. The large amount of sand within the LFA 2 unit, which was likely to have been deposited mainly during interstadial conditions between MIS 5c and MIS 5a, could partly be explained by re-deposition of reworked Molasse material. This is similar to the observations by Preusser and Schlüchter (2004), who suggest that the sandy material in the western part of the Swiss Plateau, which was deposited during the last interglacial period (Eemian, MIS 5e), could be explained by weathering and erosion of Molasse bedrock.

The coarsening upward sequence of the overlying and, therefore, younger LFA 3 at MÜN and FIH-N is interpreted as resulting from a larger sediment and water supply. Although no evidence for a direct ice contact was encountered within this unit, we infer that this unit recorded the second advance of the Valais Glacier on the Swiss plateau during the Birrfeld Glaciation. We sustain this interpretation by (i) the coarse-grained nature of the LFA 3 units at MÜN and FIH-N, (ii) the NE-directed sediment transport, and the (iii) the OSL age of 76.0 ± 6.0 ka (Preusser et al., 2007) that suggests that this unit was most likely deposited during the relatively cold period MIS 4 (Fig. 10b). In support of this interpretation, Preusser et al. (2007) described the occurrence of a residual till in the FIH pit close to the site where the OSL age was established. These authors considered this till to have been condensed to a boulder lag and to record a glacial advance into the lowlands during MIS 4. The presence of a large erratic boulder of Allalin gabbro in the till, as reported by Preusser et al. (2007) apparently confirms the interpretation of an ice contact and the origin of the sediment from the Valais during these times (Preusser et al., 2007). However, we have not found a sedimentary layer within LFA 3, which we could interpret as a glacial till. Accordingly, in case that such a sedimentary layer was indeed deposited, then it most likely had a low preservation potential and was eroded during the subsequent advance of the LGM Valais Glacier. In either case, the occurrence of gravel deposits that were deposited by a braided stream most likely during MIS 4 suggests that this archive chronicles a second possible advance of the Valais Glacier towards the foreland.

The third and possibly most extensive advance of the Alpine glaciers occurred during the LGM. In this context, we consider that: (i) the LFAs 3, 4 and 5 at FIH-S, (ii) the LFAs 4 and 5 at FIH-N, and (i) the till at MÜN (also LFA 5) were deposited during the advance (LFAs 3 and 4) and final extension (LFA 5) particularly of the Valais Glacier. Such a scenario is consistent with the chronological data established for LFA 4 in the northern part of the FIH pit, and it also corresponds to the interpretation of the Finsterhennen archives by Preusser et al. (2007). Furthermore, we interpret that the extent of the Valais Glacier was greater during the LGM than during MIS 4 and MIS 5d. We particularly base this interpretation on the large contribution of dark-coloured limestone clasts in the sediments recording the LGM advance. These clasts could have been derived from the northern part of the Alps where such a lithology is largely exposed in the Penninic and Helvetic sedimentary nappes (Spicher, 1972). This suggests that glaciers with a small catchment such as the Saane Glacier could also have contributed material to the depositional site. The growth and advance of such glaciers with a relatively small basin indeed require a period of a major glaciation, which was the case during the LGM (Bini et al., 2009).

Note that we correlated the LFA 3 unit in the northern part of FIH with MIS 4 based on an OSL age of 76.0 ± 6.0 ka (Preusser et al., 2007) and because this unit shares many similarities with the LFA 3 unit at MÜN, but not with the same LFA that is exposed in the southern part of FIH. We consider this heterochronicity in the facies relationships as a document for the high sedimentary and erosional dynamics that are usually encountered in a glacial setting, and it emphasizes the complications that are associated when analysing and correlating glaciofluvial sediments. In summary, the sedimentological and chronological data yield a highly dynamic picture of

glacial advances and retreats during the past 100 ka on the Swiss Plateau, which is consistent with the results of numerical models (Seguinot et al., 2018).

7 Summary and conclusions

Considering the IRSL ages at Müntschemier and the pre-existing radiocarbon and OSL ages at Finsterhennen, the succession at the former gravel pit records significantly older deposits, even though the gravel pits are located only ca. 3.5 km away from each other. Nevertheless, both pits record a scenario where the Valais Glacier approached the research site from the SW and sourced the braided rivers with a discharge direction towards the NE. As mentioned in the introduction and suggested by several authors before (Ivy-Ochs et al., 2008; Preusser et al., 2007, 2011), three independent glacial advances probably reached the Alpine Foreland during the last (Birrfeld) glacial cycle, which are likely to be recorded in our study sites (Fig. 10b): These are (1) the first advance likely during MIS 5d (LFA 1 at MÜN), (2) a second advance during MIS 4 (LFA 3 at MÜN and FIH-N, and (3) a third one during MIS 2, corresponding to the LGM (LFA 3, LFA 4, and LFA 5 in FIH-S, LFA 4 and LFA 5 in FIH-N, and LFA 5 at MÜN; Fig. 10b). The missing ice contact, related to the first and second glacial advances, the lower thicknesses of the gravel beds in comparison to the LGM gravels and particularly the absence of material from smaller glaciers imply that these former glaciations were probably less pronounced in this area than the LGM glaciation (Fig. 10b). According to the petrographic investigations, the first and second glacial advances were probably associated with a larger sediment supply from the southern Valaisan Alps, whereas the LGM advance was characterised by a substantial material supply from both the Valais and the catchment of the Saane Glacier. This might confirm the interpretation that the LGM advance was more extensive and therefore also recorded a petrologic signal of lower-elevated catchments. Finally, this study documents that correlations of gravel layers are complicated by the high dynamics of erosional and sedimentary processes that are usually associated with the construction (and erosion) of Quaternary sediments in Alpine forelands.

Acknowledgements
Special thanks go to Peter Thomet for guiding through the study area, and Christian Schlüchter for providing previous research material. Many thanks to the Gugger Kies und Immobilien AG and Vigier Beton Nordwest for giving access the gravel pits at any time.

Authors' contributions
FS and NA designed the study. JP conducted the analysis, drafted the figures and wrote the paper together with FS. JP, NG and ES conducted the luminescence dating, and PG contributed to the sedimentological characterization of the deposits. All co-author significantly contributed to the finalization of the text. All authors read and approved the final manuscript.

Funding
This research has been funded through the University of Bern.

Availability of data and materials
All material that has been used in this work has been presented in the figures and tables.

Declarations

Ethics approval and consent to participate
Not applicable.

Consent for publication
Not applicable.

Competing interests
The authors declare that they have no financial and competing interests.

Author details
[1]Institute of Geological Sciences, University of Bern, Baltzerstrasse 1+3, 3012 Bern, Switzerland. [2]Imperial College London, South Kensington, London SW7 2AZ, UK.

Received: 23 December 2021 Accepted: 14 February 2022
Published online: 26 March 2022

References

Aitken, M. J. (1998). *An introduction to optical dating*. Oxford University Press.
Auclair, M., Lamothe, M., & Huot, S. (2003). Measurement of anomalous fading for feldspar IRSL using SAR. *Radiatiation Measurements, 37*, 487–492. https://doi.org/10.1016/S1350-4487(03)00018-0.
Balescu, S., & Lamothe, M. (1994). Comparison of TL and IRSL age estimates of feldspar coarse grains from waterlain sediments. *Quaternary Science Review., 13*, 437–444. https://doi.org/10.1016/0277-3791(94)90056-6.
Bini, A., Buoncristiani, J.F., Couterrand, S., Ellwanger, D., Felber, M., Florineth, D., Graf, H.R., Keller, O., Kelly, M., Schlüchter, C., & Schoeneich, P. (2009). Die Schweiz während des letzteiszeitlichen Maximums (LGM): 1:500 000, Bundesamt für Landestopografie, swisstopo. Wabern, Switzerland.
Boulton, G. S. (1978). Boulder shapes and grain-size distributions of debris as indicators of transport paths through a glacier and till genesis. *Sedimentology, 25*, 773–799. https://doi.org/10.1111/j.1365-3091.1978.tb00329.x.
Buechi, M. W., Frank, S. M., Graf, H. R., Menzies, J., & Anselmetti, F. S. (2017). Subglacial emplacement of tills and meltwater deposits at the base of overdeepened bedrock troughs. *Sedimentology, 64*, 658–685. https://doi.org/10.1111/sed.12319.
Cailleux, A. (1947). L'indice d'émoussé; définition et première application, Sociéeé Géologique de France.
Claude, A., Akçar, N., Ivy-Ochs, S. D., Schlunegger, F., Kubík, P. W., Dehnert, A., Kuhlemann, J., Rahn, M., & Schlüchter, C. (2017a). Timing of early Quaternary gravel accumulation in the Swiss Alpine Foreland. *Geomorphology, 276*, 71–85. https://doi.org/10.1016/j.geomorph.2016.10.016.
Claude, A., Akçar, N., Ivy-Ochs, S., Schlunegger, F., Rentzel, P., Pümpin, C., Tikhomirov, D., Kubik, P. W., Vockenhuber, C., Dehnert, A., Rahn, M., & Schlüchter, C. (2017b). Chronology of Quaternary terrace deposits at the locality Hohle Gasse (Pratteln, NW Switzerland). *Swiss Journal of Geosciences, 110*, 793–809. https://doi.org/10.1007/s00015-017-0278-z.
Claude, A., Akçar, N., Ivy-Ochs, S., Schlunegger, F., Kubik, P. W., Christl, M., Vockenhuber, C., Kuhlemann, J., Rahn, M., & Schlüchter, C. (2019). Changes in landscape evolution patterns in the northern Swiss Alpine Foreland during the mid-Pleistocene revolution. *GSA Bulletin, 131*, 11–12. https://doi.org/10.1130/B31880.1.
Dehnert, A., Lowick, S. E., Preusser, F., Anselmetti, F. S., Drescher-Schneider, R., Graf, H. R., Heller, F., Horstmeyer, H., Kemna, H. A., Nowaczyk, N. R., Züger, A., & Furrer, H. (2012). Evolution of an overdeepened trough in the

northern Alpine Foreland at Niederweningen, Switzerland. *Quaternary Sciences Reviews, 34*, 127–145. https://doi.org/10.1016/j.quascirev.2011.12.015.
Doeglas, D. J. (1962). The structure of sedimentary deposits of braided rivers. *Sedimentology, 1*, 167–190. https://doi.org/10.1111/j.1365-3091.1962.tb00453.x.
Du Pasquier, L. (1891). *Über die Fluvioglacialen Ablagerungen der Nordschweiz (ausserhalb der inneren Moränenzonen)*. Schmid Francke.
Durcan, J. A., King, G. E., & Duller, G. A. T. (2015). DRAC: Dose rate and age calculator for trapped charge dating. *Quaternary Geochronology, 28*, 54–61. https://doi.org/10.1016/j.quageo.2015.03.012.
Dürst Stucki, M., & Schlunegger, F. (2013). Identification of erosional mechanisms during past glaciations based on a bedrock surface model of the central European Alps. *Earth and Planetary Sciences Letters, 384*, 57–70. https://doi.org/10.1016/j.epsl.2013.10.009.
Etienne, J. L., Glasser, N. F., & Hambrey, M. J. (2003). Proglacial sediment-landform associations of a polythermal glacier: Storglaciären, Northern Sweden. *Geografiska Annaler, 85*, 149–164.
Eugster, W., & Schneider, S. (2006). Auswirkungen der Landnutzungsänderung auf das regionale Klima: das Typbeispiel Juragewässerkorrektion. In: GrenzWerte, Tagungsbericht und wissenschaftliche Abhandlungen des 55. Deutschen Geographentags, Trier, 2005. pp. 553–560.
Evans, D. J. A., & Benn, D. I. (2014). *A practical guide to the study of glacial sediments*. Routledge.
Evans, D. J. A., Phillips, E. R., Hiemstra, J. F., & Auton, C. A. (2006). Subglacial till: Formation, sedimentary characteristics and classification. *Earth-Science Reviews, 78*, 115–176. https://doi.org/10.1016/j.earscirev.2006.04.001.
Fuchs, M., & Owen, L. A. (2008). Luminescence dating of glacial and associated sediments: Review, recommendations and future directions. *Boreas, 37*, 636–659. https://doi.org/10.1111/j.1502-3885.2008.00052.x.
Gaar, D., Graf, H. R., & Preusser, F. (2019). New chronological constraints on the timing of Late Pleistocene glacier advances in northern Switzerland. *Journal of Quaternary Sciences, 68*, 53–73. https://doi.org/10.5194/egqsj-68-53-2019.
Gaar, D., Lowick, S. E., & Preusser, F. (2014). Performance of different luminescence approaches for the dating of known-age glaciofluvial deposits from Northern Switzerland. *Geochronometria, 41*, 65–80. https://doi.org/10.2478/s13386-013-0139-0.
Galbraith, R. F., & Green, P. F. (1990). Estimating the component ages in a finite mixture. *International Journal of Radiation Applicaltions and Instrumentation, 17*, 197–206. https://doi.org/10.1016/1359-0189(90)90035-V.
Galbraith, R. F., & Roberts, R. G. (2012). Statistical aspects of equivalent dose and error calculation and display in OSL dating: An overview and some recommendations. *Quaternary Geochronology, 11*, 1–27. https://doi.org/10.1016/j.quageo.2012.04.020.
Gegg, L., Deplazes, G., Keller, L., Madritsch, H., Spillmann, T., Anselmetti, F. S., & Buechi, M. W. (2021). 3D morphology of a glacially overdeepened trough controlled by underlying bedrock geology. *Geomorphology, 394*, 107950. https://doi.org/10.1016/j.geomorph.2021.107950.
Gerth, A., & Becker-Haumann, R. (2007). Sedimentuntersuchungen an unterpleistozänen Schmelzwasserablagerungen und Periglazialschottern im Riß-Iller-Gebiet, deutsches Alpenvorland. *E&G Quaternary Science Journal, 56*, 186–211. https://doi.org/10.3285/eg.56.3.04.
Graf, H.R. (2009a). Stratigraphie von Mittel- und Spätpleistozän in der Nordschweiz. – Beiträge zur Geologischen Karte der Schweiz, 168. Bundesamt für Landestopografie swisstopo, Wabern.
Graf, H. R. (2009b). Stratigrafie und Morphogenese von frühpleistozänen Ablagerungen zwischen Bodensee und Klettgau. *Journal of Quaternary Sciences, 58*, 12–54.
Graf, H. R., & Müller, B. (1999). Das Quartär: Die Epoche der Eiszeiten. In Th. Bolliger (Ed.), *Geologie des Kantons Zürich* (pp. 71–95). Ott Verlag.
Graf, A., Akçar, N., Ivy-Ochs, S., Strasky, S., Kubik, P. W., Christl, M., Burkhard, M., Wieler, R., & Schlüchter, C. (2015). Multiple advances of Alpine glaciers into the Jura Mountains in the Northwestern Switzerland. *Swiss Journal of Geosciences, 108*, 225–238. https://doi.org/10.1007/s00015-015-0195-y.
Gribenski, N., Valla, P. G., Preusser, F., Roattino, T., Crouzet, C., & Buoncristiani, J. F. (2021). Out-of-phase Late Pleistocene glacial maxima in the Western Alps reflect past changes in North Atlantic atmospheric circulation. *Geology, 49*, 1096–1101. https://doi.org/10.1130/G48688.1.
Hart, J. K., & Boulton, G. S. (1991). The interrelation of glaciotectonic and glaciodepositional processes within the glacial environment. *Quaternary Science Reviews, 10*, 335–350. https://doi.org/10.1016/0277-3791(91)90035-S.
Helmens, K. F. (2014). The last interglacial-glacial cycle (MIS 5–2) re-examined based on long proxy records from central and northern europe. *Quaternary Sciences Reviews, 86*, 115–143. https://doi.org/10.1016/j.quascirev.2013.12.012.
Huntley, D. J., & Baril, M. R. (1997). The K content of the K-feldspars being measured in optical dating or in thermoluminescence dating. *Ancient TL, 15*, 11–13.
Huntley, D. J., & Lamothe, M. (2001). Ubiquity of anomalous fading in K-feldspars and the measurement and correction for it in optical dating. *Canadian Journal of Earth Sciences, 38*, 1093–1106. https://doi.org/10.1139/cjes-38-7-1093.
Ivy-Ochs, S., Kerschner, H., Reuther, A., Preusser, F., Heine, K., Maisch, M., Kubik, P. W., & Schlüchter, C. (2008). Chonology of the last glacial cycle in the European Alps. *Journal of Quaternary Sciences, 23*, 559–573. https://doi.org/10.1002/jqs.1202.
Johansson, L. E. (1963). Orientation of pebbles in running water. A laboratory study. *Geografiska Annaler, 45*, 85–112.
Kars, R. H., Reimann, T., Ankjærgaard, C., & Jakob, W. (2014). Bleaching of the post-IR IRSL signal: new insights for feldsparluminescence dating. *Boreas, 43*, 780–791. https://doi.org/10.1111/bor.12082.
Kauffman, M. E., & Ritter, D. F. (1981). Cobble imbrication as a sensitive indicator of subtle local changes in river flow direction. *Geology, 9*, 299–302.
Kelling, G., & Williams, P. F. (1967). Flume studies of the reorientation of pebbles and shells. *Journal of Geology, 75*, 243–267.
Kreutzer, S., Schmidt, C., Fuchs, M., Dietze, M., Fischer, M., & Fuchs, M. (2012). Introducing an R package for luminescence dating analysis. *Ancient TL, 30*, 1–8.
Krumbein, W. C. (1939). Preferred orientation of pebbles in sedimentary deposits. *Journal of Geololgy, 47*, 673–706.
Lukas, S., Benn, D. I., Boston, C. M., Brook, M., Coray, S., Evans, D. J. A., Graf, A., Kellerer-Pirklbauer, A., Kirkbride, M. P., Krabbendam, M., Lovell, H., Machiedo, M., Mills, S. C., Nye, K., Reinardy, B. T. I., Ross, F. H., & Signer, M. (2013). Clast shape analysis and clast transport paths in glacial environments: A critical review of methods and the role of lithology. *Earth-Science Reviews, 121*, 96–116. https://doi.org/10.1016/j.earscirev.2013.02.005.
Magrani, F., Valla, P. G., Gribenski, N., & Serra, E. (2020). Glacial overdeepenings in the Swiss Alps and foreland: Spatial distribution and morphometrics. *Quaternary Sciences Reviews, 243*, 106483. https://doi.org/10.1016/j.quascirev.2020.106483.
Martinson, D. G., Pisias, N. G., Hays, J. D., Imbrie, J., Moore, T. C., & Shackleton, N. J. (1987). Age dating and the orbital theory of the ice ages: Development of a high-resolution 0 to 300,000-year chronostratigraphy. *Quaternary Research, 27*, 1–29. https://doi.org/10.1016/0033-5894(87)90046-9.
Matter, A. (1964). Sedimentologische Untersuchungen im östlichen Napfgebiet (Entlebuch - Tal der Grossen Fontanne, Kt. Luzern). *Eclogae Geologicae Helvetiae, 57*, 315–329. https://doi.org/10.5169/seals-163142.
Meichtry, N. (2016). Last deglaciation of the Aare valley. Unpublished Ms Thesis. Bern, Switzerland.
Miall, A. D. (1977). A review of the braided-river depositional environment. *Earth-Sciences Reviews., 13*, 1–62. https://doi.org/10.1016/0012-8252(77)90055-1.
Miall, A. D. (1978). Lithofacies types and vertical profile models in braided river deposits: A summary. *Fluvial Sedimentolology, 5*, 597–604.
Miall, A. D. (1985). Architectural-element analysis: A new method of facies analysis applied to fluvial deposits. *Earth-Sciences Reviews, 22*, 261–308. https://doi.org/10.1016/0012-8252(85)90001-7.
Millane, R. P., Weir, M. I., & Smart, G. M. (2006). Automated analysis of imbrication and flow direction in alluvial sediments using laser-scan data. *Journal of Sedimentary Research, 76*, 1049–1055. https://doi.org/10.2110/jsr.2006.098.
Monegato, G., & Ravazzi, C. (2018). The Late Pleistocene multifold glaciation in the Alps: Updates and open questions. *Alpine and Mediterranean Quaternary, 31*, 225–229. https://doi.org/10.26382/AIQUA.2018.AIQUA conference.
Muttoni, G., Carcano, C., Garzanti, E., Ghielmi, M., Piccin, A., Pini, R., Rogledi, S., & Sciunnach, D. (2003). Onset of major Pleistocene glaciations in the Alps. *Geology, 31*, 989–992. https://doi.org/10.1130/G19445.1.

Nichols, G. (2009). *Sedimentology and stratigraphy*. Wiley-Blackwell.
Potter, P. E., & Pettijohn, F. J. (1977). Paleocurrents and basin analysis. *Springer-Verlag*. https://doi.org/10.1180/minmag.1979.043.325.36.
Preusser, F. (1999). Luminescence dating of fluvial sediments and overbank deposits from Gossau, Switzerland: Fine grain dating. *Quaternary Geochronology, 18*, 217–222. https://doi.org/10.1016/S0277-3791(98)00054-7.
Preusser, F. (2004). Towards a chronology of the Late Pleistocene in the northern Alpine Foreland. *Boreas, 33*, 195–210. https://doi.org/10.1080/03009480410001271.
Preusser, F., Blei, A., Graf, H., & Schlüchter, C. (2007). Luminescene dating of Würmian (Weichselian) proglacial sediments from Switzerland: Methodological aspects and stratigraphical conclusions. *Boreas, 36*, 130–142. https://doi.org/10.1080/03009480600923378.
Preusser, F., Graf, H. R., Keller, O., Krayss, E., & Schlüchter, C. (2011). Quaternary glaciation history of northern Switzerland. *Journal of Quaternary Sciences, 60*, 282–305. https://doi.org/10.3285/eg.60.2-3.06.
Preusser, F., Kasper, H., & Preusser, F. (2001). Comparison of dose rate determination using high-resolution gamma spectrometry and inductively coupled plasma-mass spectrometry. *Ancient TL, 19*, 19–23.
Preusser, F., & Schlüchter, C. (2004). Dates from an important early Late Pleistocene ice advance in the Aare valley, Switzerland. *Eclogae Geologicae Helvetiae, 97*, 245–253. https://doi.org/10.1007/s00015-004-1119-4.
Reber, R., & Schlunegger, F. (2016). Unravelling the moisture sources of the Alpine glaciers using tunnel valleys as constraints. *Terra Nova, 28*, 202–211. https://doi.org/10.1111/ter.12211.
Reimann, T., & Tsukamoto S. (2012). Dating the recent past (<500 years) by post-IR IRSL feldspar - Examples from the North Sea and Baltic Sea coast. *Quaternary Geochronology*, *10*, 180–187. https://doi.org/10.1016/j.quageo.2012.04.011.
Rust, B. R. (1972). Pebble orientation in fluvial sediments. *Journal of Sedimentary Petrology, 42*, 384–388. https://doi.org/10.1306/74d7255e-2b21-11d7-8648000102c1865d
Rust, B. R. (1978). Depositional models for braided alluvium. *Canadian Society of Petroleum Geologists, 5*, 605–625.
Schiemenz, S. (1960). Fazies und Paläogeographie der subalpinen Molasse zwischen Bodensee und Isar. *Beihefte Zum Geologischen Jahrbuch, 38*, 1–119.
Schlee, J. S. (1957). Fluvial gravel fabric. *Journal of Sedimentary Research., 27*, 162–176. https://doi.org/10.1306/74D7068C-2B21-11D7-8648000102C1865D
Schlüchter, C. (1976). Geologische Untersuchungen im Quartär des Aaretals südlich von Bern. Beiträge zur Geol. Karte der Schweiz NF148.
Schlüchter, C. (1986). The Quaternary glaciations of Switzerland, with special reference to the Northern Alpine Foreland. *Quaternary-Science Reviews., 5*, 413–419. https://doi.org/10.1016/0277-3791(86)90206-4
Schlüchter, C. (1989). Eiszeitliche Lockergesteine—Geologie, Genese und Eigenschaften. Habilitationsschrift, ETH Zürich, Switzerland.
Schlüchter, C. (2004). The Swiss glacial record—a schematic summary. *Quaternary Sciences, 2*, 413–418. https://doi.org/10.1016/S1571-0866(04)80092-7
Schlüchter, C., Akçar, N., & Ivy-Ochs, S. (2021). *The quaternary period in Switzerland*. Springer International Publishing. https://doi.org/10.1007/978-3-030-43203-4_4
Schlunegger, F., & Garefalakis, P. (2018). Clast imbrication in coarse-grained mountain streams and stratigraphic archives as indicator of deposition in upper flow regime conditions. *Earth Surface Dynamics, 6*, 743–761. https://doi.org/10.5194/esurf-6-743-2018
Schlunegger, F., Matter, A., & Mange, M. A. (1993). Alluvial fan sedimentation and structure of the southern Molasse Basin margin, Lake Thun area, Switzerland. *Eclogae Geologicae Helvetiae, 86*, 717–750.
Schwenk, M., Schläfli, P., Bandou, D., Gribenski, N., Douillet, G.A., & Schlunegger, F. (2022). From glacial erosion to basin overfill: A 240 m-thick overdeepening–fill sequence in Bern, Switzerland. *Scientific Drilling*, 30, in press.
Seguinot, J., Ivy-Ochs, S., Jouvet, G., Huss, M., Fink, M., & Preusser, F. (2018). Modelling last glacial cycle ice dynamics in the Alps. *The Cryosphere, 12*, 3265–3285. https://doi.org/10.5194/tc-12-3265-2018
Shackleton, N. J., Chapman, M., Sánchez-Goni, M. F., Pailler, D., & Lancelot, Y. (2002). The classic marine isotope substage 5e. *Quaternary Research, 58*, 14–16. https://doi.org/10.1006/qres.2001.2312
Shakun, J. D., & Carlson, A. E. (2010). A global perspective on Last Glacial Maximum to Holocene climate change. *Quaternary Science Reviews, 29*, 1801–1816. https://doi.org/10.1016/j.quascirev.2010.03.016
Spicher, A. (1972). *Tektonische Karte der Schweiz*. Schweizerische Geologische Kommission.
van der Meer, J. J. M. (1993). Microscopic evidence of subglacial deformation. *Quaternary Science Reviews, 12*, 553–587. https://doi.org/10.1016/0277-3791(93)90069-X
Weltje, G. J., & von Eynatten, H. (2004). Quantitative provenance analysis of sediments: Review and outlook. *Sedimentary Geology, 171*, 1–11. https://doi.org/10.1016/j.sedgeo.2004.05.007
Wintle, A. G. (1973). Anomalous fading of thermo- luminescence in mineral samples. *Nature, 245*, 143–144.
Wintle, A. G., & Murray, A. S. (2006). A review of quartz optically stimulated luminescence characteristics and their relevance in single-aliquot regeneration dating protocols. *Radiatiation Measurements, 41*, 369–391. https://doi.org/10.1016/j.radmeas.2005.11.001
Wohlfarth, B. (2013). A review of Early Weichselian climate (MIS 5d-a) in Europe. Technical report/Svensk kärnbränslehantering AB, 2013, Stockholm.

Publisher's Note